論文 / 著書情報
Article / Book Information

題目(和文)	複数の環状RGDペプチドを担持したポリマーコンジュゲート型汎用性腫瘍標的リガンド分子の開発と光増感剤デリバリーへの応用
Title(English)	Development of polymer conjugates having multiple cyclic RGD peptides as versatile ligand molecules to target malignant tumors and its application in delivery of photosensitizers and nucleic acids
著者(和文)	DouXuebo
Author(English)	Xuebo Dou
出典(和文)	学位:博士(工学), 学位授与機関:東京工業大学, 報告番号:甲第11111号, 授与年月日:2019年3月26日, 学位の種別:課程博士, 審査員:西山 伸宏,小畠 英理,中村 浩之,宍戸 厚,田巻 孝敬
Citation(English)	Degree:Doctor (Engineering), Conferring organization: Tokyo Institute of Technology, Report number:甲第11111号, Conferred date:2019/3/26, Degree Type:Course doctor, Examiner:,,,,
学位種別(和文)	博士論文
Type(English)	Doctoral Thesis

Doctoral thesis

Development of polymer conjugates having multiple cyclic RGD peptides as versatile ligand molecules to target malignant tumors and its application in delivery of photosensitizers and nucleic acids

複数の環状RGDペプチドを担持したポリマーコンジュゲート型汎用性腫瘍標的リガンド分子の開発と光増感剤・核酸デリバリーへの応用

Dou Xuebo

Table of contents

Chapter 1 Introduction 1
1.1 General introduction 2
1.2 Principle of photodynamic therapy 3
1.2.1 Photodynamic Reaction 3
1.2.2Mechanism of Tumor Destruction 3
1.2.3 Direct tumor-cell Damage 4
1.2.4 Vascular damage. 5
1.2.5 Immune response. 5
1.3 Photosensitizers 7
1.3.1 The first generation PS 10
1.3.2 The second generation PS 11
1.3.3 The third generation PS 14
1.4 Current limitations of photodynamic therapy 14
1.5 Delivery system of PS 16
1.5.1 Organic Nanoparticles 18
Liposomes 18
Polyester and Polyacrylamide Based Nanoparticles. 19
Dendrimer Based Nanoparticles. 20
1.5.2 Nonbiodegradable Nanoparticles. 21
Silica Nanoparticles. 21
Gold Nanoparticles. 22
Magnetic Nanoparticle 23
1.5.3 Photosensitizer-antibody conjugates 23
1.6 Future directions 24
1.7 Significance of This Study 25
1.8 Outline of the Dissertation 26
Chapter 2. Synthesis of PS polymer conjugates 28

2.1 Introduction 29
2.2 Materials and Methods 31
2.2.1 Materials 31
2.2.2 Synthesis of azide-PEG-NH_2 32
2.2.3 Synthesis of azide-PEG-poly(L-glutamic acid) (PEG-PGlu) 33
2.2.4 Synthesis of cRGD-functionalized PEG-PGlu (azide-PEG-P[Glu/Glu(cRGD)]) and cRAD-functionalized PEG-PGlu (azide-PEG-P[Glu/Glu(cRAD)]) 35
2.2.5. Synthesis of 700DX-PEG-PGlu-cRGDx and 700DX-PEG-PGlu-cRAD15 37
2.2.6. Synthesis of 700DX-PEG-cRGD (700DX -PEG-cRGD) 39
2.3 Results and Discussion 40
3. Biological activities of PS-polymer conjugates 49
3.1 Introduction 50
3.2 Materials and Methods 51
3.2.1 Materials 51
3.2.2 Cell Culture 51
3.2.3 Cellular uptake 51
3.2.4 Confocal laser scanning microscopic observation of subcellular distribution 52
3.2.5 Cell viability 52
3.2.6 Biodistribution study 53
3.2.7 Microscopic observation of intratumoral distribution 53
3.2.8 In vivo antitumor activity 54
3.3 Results and Discussion 54
3.3.1 Cellular uptake and subcellular distribution 54
3.3.2 Cell viability assay 57
3.3.3 Biodistribution 60
3.3.4 Intratumoral distribution 63

3.3.5. In vivo antitumor activity....65
Conclusion....67
4. Photochemical internalization application for siRNA delivery system....68
4.1 Introduction....69
4.2 Materials and Methods....70
4.2.1 Materials....70
4.2.2 Cell lines....70
4.2.3 Cell viability and Transfection assay....70
4.2.4 Fluorescence Microscopy....71
Results and Discussion....72
4.3.1 PCI....72
Chapter 5. Summary of the Dissertation....78
5.1 Summary of the Dissertation....79
5.2 Future perspectives....80
References....82
Achievements....103

Chapter 1 Introduction

1.1 General introduction

Photodynamic therapy (PDT) was developed in the last century after some agents inducing cell death in the presence of light were found. The discovery of 'photodynamic action' phenomenon at the beginning of the 20th century promoted the establishment of modern PDT. PDT is a treatment that uses a non-toxic drug, called a photosensitizer (PS), and a particular type of light. After activated by a specific wavelength of light, PSs generate reactive oxygen species (ROS) which have huge cytotoxicity. Since travel distance of ROS in PDT is several ten nanometers in cells, the cytotoxicity of the activated photosensitize are only in the particular areas of tissue that have been exposed to light. Therefore, PDT does not have the disadvantages, such as systemic side effects, which are often associated with chemotherapy. Different from the radiation therapy, PDT is not limited by the cumulative radiation dose, because the light applied in PDT has no toxicity. Compared to the chemotherapy, radiation therapy, and surgery, PDT has other advantages like minimal invasiveness, excellent antitumor effect, and improvement of the patients' life quality. Because of these advantages, PDT, treated as a safe and potent alternate treatment, has been receiving greater attention in recent years and has now become an essential field in medical research. Since Thomas Dougherty successfully treated skin cancer in patients by PDT, many PSs have been developed and could be classified into three generation. Some of them have received official approval around the world. Over the past decades, PDT has shown the high anticancer effect on several cancers, such as superficial bladder cancers[1], early and obstructive lung cancers[2], head and neck cancers[3-5], breast cancers[6-8], gynaecological tumors[9-11], intraocular tumors[12-14], brain tumors[15-18], colorectal cancer[19,20], cutaneous malignancies[21-23], intraperitoneal tumors[24], mesotheliomas[25], cholangiocarcinomas[26] and pancreatic cancers[27]. Besides directly destroying the tumor, PDT has also been used as adjunctive therapy to reduce residual tumor burden after surgical resection[28-31]. Although significant progress has been made in PDT, its clinic application was still

limited by the lack of ideal PSs, choosing and delivering the light and difficulties in planning the treatment and monitoring the treatment response. In the following parts, the principle of photodynamic therapy, photosensitizers, current limitations, the delivery system of PS and future directions will be introduced in detail.

1.2 Principle of photodynamic therapy

1.2.1 Photodynamic Reaction

After absorbing the light (photons), PS at ground state (singlet state) will transfer into a temporary excited singlet state. Some part of the excited PS will emit fluorescence and transfer back to the ground state. The other part will further transfer to a relatively permanent electronically excited state (triplet state)[32]. The triplet excited PS can then directly interact with a substrate, such as the cell membrane or biomolecules, and transfer a proton or an electron to form a radical anion or cation, respectively, which then reacts with oxygen to produce oxygenated products such as superoxide anion radicals, hydroxyl radicals, and hydrogen peroxides (type I reaction). Alternatively, the energy of the excited PS can be directly transferred to oxygen, to form $^1O_2$, a highly reactive ROS (type II reaction). Attributed to the high reactivity, ROS could rapidly attack surrounding organic compounds to create cytotoxicity. It is believed that $^1O_2$ gives the best contribution to the PDT.[33] Both type I and type II reactions occurred simultaneously and depending on the existence of oxygen, so the concentrations of molecular oxygen heavily influence the two types of reactions.

1.2.2Mechanism of Tumor Destruction

It is well known that direct tumor cell damage, tumor-associated vasculature damage, and inflammatory and immune response are the three main mechanisms of antitumor effect of PDT.[34] During PDT, tumor cells get the damage from the ROS and are killed

directly. The tumor-associated vasculatures also get the damage and are shut down. The surviving tumor cells can be dead because of the lack of nutrients and oxygen. PDT can also activate the immune response to kill tumor cells. These mechanisms affect each other and could be found in every PDT; however, the importance of each mechanism in specific PDT is different. Even the relationship between these mechanisms has not been clear, but the combination of them is known as an essential factor for achieving a long-term tumor control.

1.2.3 Direct tumor-cell Damage.

ROS has high reactivity, leading to the very short life and restricted diffusion distance of ROS in biological systems. These characteristics decide that the tumor cell damage can be co-localized with the distribution of PS. After cell uptake, the PS induces irreversible damage to the vital subcellular targets such as plasma membrane and organelles like mitochondria, lysosomes, Golgi apparatus, and endoplasmic reticulum (ER) by generating ROS to oxidize the biomolecules of these organelles. The intracellular distribution of PS was decided by its structural features such as hydrophobicity and charges. It was rarely reported that there are mutations during PDT because most of PS do not accumulate in cell nuclei. Direct tumor cell death can be classified as apoptosis, necrosis, and autophagy.[35] In in vivo experiment, PDT could decrease the tumor cells and inhibit the growth of the tumor. However, the eradication of the tumor is sometimes difficult to be achieved, which is mostly caused by the heterogeneous distribution of PS in the tumor. The local concentration in the deep part of the tumor was not high enough to produce the necessary toxicity. Photodynamic reaction is limited not only by the low concentration of PS but also by the hypoxia. There are two ways to overcome this problem. Reducing the light fluency rate to minimize oxygen consumption rate, and fractionating the PDT light delivery to allow re-oxygenation of the tissue could dissolve the problem. In conclusion, direct tumor-cell damage is the most important and the most fundamental

mechanism of PDT; however, it is sometimes not enough to cure the tumor.

1.2.4 Vascular damage.

The growth of solid tumors is supported by tumor-associated blood vessels, by which oxygen and nutrients are delivered. At the same time, the tumor also induces the growth of tumor-associated blood vessels (angiogenesis); the growth of the tumor and blood vessels promote each other. This mutual improvement led to the uncontrolled growth of the tumor; therefore, blocking it by giving the damage to vasculature is one promising approach to inhibit the growth of the tumor. When the PS localized in endothelial cells or the vessel walls is activated, the endothelial cells will get the damage from ROS. The PS in the blood also hurts the endothelial cells. The damaged endothelial cells will lead to the formation of thrombosis, aggregation of platelet, adhesion of leukocyte, and release of vasoactive molecules[36]. These reactions will result in partial or complete vascular shutdown which will inhibit the growth of tumor[37].

1.2.5 Immune response.

The immune response was reported in the late 1980s and early 1990s. The scientists found an interesting phenomenon that the immune cells, such as lymphocytes, leukocytes, and macrophages, will localize to the PDT-treated tissue. This phenomenon suggests that the PDT could activate the immune response. Different from direct tumor cell kill, immune response plays an essential role in the longitudinal tumor control and complete tumor response to PDT.[38] After the direct cell death, some inflammatory mediators, such as components of the complement system, proteinases, peroxidases, cytokines, growth factors, and other immuno-regulators, will be released from the tumor cells, and these factors mediate the inflammatory process. The white

blood cell components, such as dendritic cells (DCs) and neutrophils, will localize into the tumor site by perceiving these factors. After accumulation of white blood cell, damaged cancer cells were removed by phagocytosis of DCs. And proteins of these cancer cells were transferred to CD4 helper T lymphocytes to activate CD8 cytotoxic T lymphocytes by mature DCs in the regional lymph nodes. Activated CD8 T cells start the immune response. Both necrosis and apoptosis of tumor cells happens in the immune response, and inhibit the growth of tumor for a long time.

1.3 Photosensitizers

Properties of PS seriously affect the therapeutic effect of PDT. Although selectivity offered by the introduction of light, an ideal PS should also provide the tumor selectivity. For reducing the side effect on non-target tissues, low dark toxicity and rapid clearance from the body post-procedure of PS were required[39]. Suitable photophysical characteristics such as high quantum yield of triplet state formation, appropriate triplet lifetime to interact with ground state oxygen, and strong photochemical stability (to prevent degradation of the photosensitizer) are prerequisites for efficient and stable generation of ROS. Amphilicity is another property for a clinically successful PS. In systemic administration, some degree of hydrophilicity was required for unhindered delivery to the target tissue (tumor), and some degree of lipophilicity was required for the binding to the target cells. For intravenous administration, PS should be soluble in biological media. For the hydrophobic PS, a hydrophilic delivery system must be established to transport the PS to the target site via the bloodstream. Since tissue penetration of light increased with its wavelengths, longer wavelengths allow the light to penetrate deeper and treat larger structures which are significant for PDT for cancer. The PS must be activated by wavelengths of light above 700 nm. Also, a PS should ideally be a single pure compound to allow manufacturing under good manufacturing practice (GMP) conditions with quality control and low manufacturing costs, and leading to better stability in storage. It is difficult to find any natural substances or develop any chemical synthesis reagents that can meet all of the above requirements. However many first and second generation PSs that only satisfy some requirements have been approved for clinical use or being tested in clinical trials (table 1). The first generation PS, hematoporphyrin derivative, is approved in over 40 countries. But the patients treated with it should avoid light several weeks after treatment, because of retention of the PSs in the healthy tissue and skin. Another PS, phenyl chlorine (mTHPC), is approved for treatment of head and neck, prostate and pancreatic tumors in Europe.

However, it still has some drawbacks, like skin photosensitivity and poor water solubility. Hence the development of new photosensitizers will improve the prospects for the use of PDT.

Table 1. List of approved for Clinical Use/under Clinical Trials Photosensitizers

Class	PS	Trade Name	Potential indication	Current status	Typical maximum absorption(nm)
Hematoporphyrin	HpD	Photofrin	Endobronchial non-small-cell lung cancer, esophahgeal cancers, bladder vcancer, gastric cancer and cervical cancer	Approved in more than 40 countries	630
	HpD	phorogem			630
Protoporphyrin prodrugs	5-Aminolevulinic Acid (5-ALA)	Levulan	Basal-cell carcinoma, head and neck and gynaecological tumors	Approved in USA and Europe	635
	5-ALA-hexylester/H-ALA	Hexvix	Bladder tumors	Approved in USA	~400
	5-ALA-methylester/ M-ALA	Metvixia	Basal-cell carcinoma	Approved in USA, Europe, New Zealand and Australia	635
	5-ALA-Benzylester	Benzvix	Gastrointestinal cancer		635
Chlorins	Meta-tetrahydroxyphenylchlorin (m-THPC)	Foscan	head and neck, prostate and pancreatic tumors	Approved in Europe	652
	Mono-L-aspartyl chlorin e6	Laserphyrin	Lung cancer and solid tumors from diverse origins	Approved in Japan	664
Phthalocyanines	Sulfonated aluminium phthalocyanines	Photosens	Various cancers	Approved in Russia	675
	Silicon phthalocyanines	Pc4	T-cell non-Hodgkin Lymphoma and skin cancers	Clinical trials(phase I)/USA	670
	Zinc phthalocyanine	CGP55847	Sin cancer	Clinical trials(phase I)/USA	675
Pheophorbide-a	HPPH	Photochlor	Early esophageal cancers, non-small cell lung cancer	Clinical trials(phase II)	665
	Palladium-bacteriopheophorbide	Tookad	Recurrent prostate cancer	Clinical trials(phase III)	763

1.3.1 The first generation PS

The first generation PS was developed from a porphyrin-based mixture called hematoporphyrin derivative (HpD). The HpD was synthesized in 1960 by Lipson and Baldes[40], and utilized for tumor imaging instead of PDT till the early 1970's[41]. After found only the higher molecular weight fraction of HpD has the potential for PDT, Photofrin™, a portion of HpD, was developed. The HpD, represented by Photofrin™, was the earliest and most useful PSs in the clinical application with advantages including high antitumor effect, negligible dark toxicity, and water solubility. These advantages promoted Photofrin™ to get the first approval in Canada in 1993. However, it exhibits some drawbacks. The wavelength of light utilized to activate Photofrin™ was only 630 nm. As mentioned above, light at this wavelength does not show high skin penetration ability. Hence the extreme penetration depth of infrared light is only 4mm, large size and these PSs could not treat the deeply-seated tumor. Low extinction coefficients lead to the requirement of a large amount of the PS for a satisfactory therapeutic effect. Another drawback was the low body clearance rate, leading to up to two or three days of the drug-light interval during which the patient must be protected from light. Moreover, the PSs could retain in the healthy tissue and skin. The continuous severe photosensitivity could last approximately 4-6 weeks after treatment, although this systemic side effects could be prevented.[42] The above drawbacks and lack of tumor selectivity have led the researchers to try to find some other agents to use as ideal PSs.

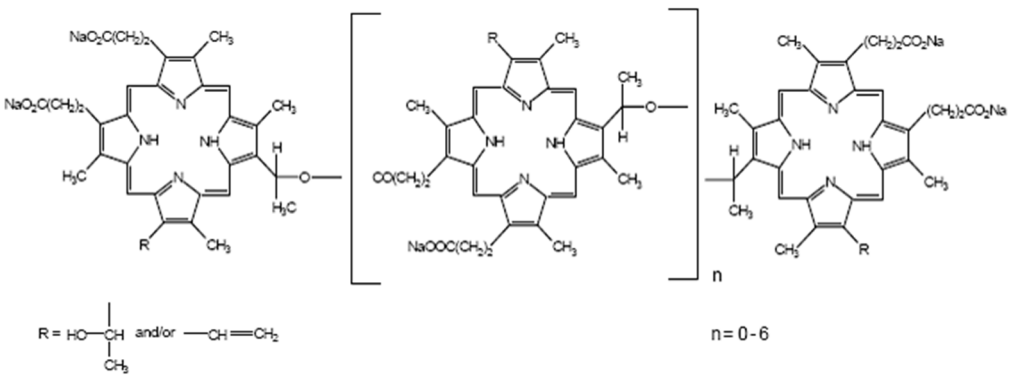

Figure 1.3.1. Structure of Photofrin

1.3.2 The second generation PS

To improve the therapeutic effect of PDT, the second generation PS was continuously developed from the 1980's. The second generation PSs could be divided into porphyrinoid compounds and non-porphyrinoid compounds. In 1984, dihydroporphyrins (chlorins), an essential part of porphyrinoid compounds, were developed by Morgan and coworkers. The wavelength of the excitation light of these agents was 690 nm. The skin penetration depth of this light was twice than that of excitation light of first-generation PSs. The other improvements were a higher yield of singlet oxygen and rapid clearance which led to only about three days skin photosensitivity. However, most of the porphyrinoid compounds and some of non-porphyrinoid compounds exhibited high hydrophobicity, caused by their chemical structure. Hydrophobic PS could more easily penetrate the cell membrane than the hydrophilic PS, but they often aggregated in aqueous solution and bio-environment, leading to the down-regulated yield of singlet oxygen and poor pharmacokinetics. Clinical applications have also been limited by low solubility in physiological solvents and body fluids[43]. Thus, hydrophilic PSs of second-generation PSs show more potential for the clinical application. Conventional methods to improve the hydrophobicity of PS are introducing the hydrophilic substituents, including sulphonic acid, carboxylic acid, hydroxy groups, quaternary ammonium salts, carbonyl groups, and pyridinium substituents, to PS structure[44]. As well as the introduction of hydrophilic groups, the hydrophilicity of PS could be improved by oxidation and/or addition of a central ion. One famous example was the mono-L-aspartyl chlorin e6 (MACE). This PS had enhanced hydrophilicity by adding four carboxylic groups to the porphyrinoid structure and kept the advantages of the chlorin family, such as high singlet oxygen production rate and the excellent absorbance at 664 nm. In a clinical study for early-stage lung cancer, it showed the safety and wonderful antitumor effect (30 complete responses in 35 patients)[45]. On the other hand, hydrophilic non-porphyrinoid compounds also shown competitiveness in

PDT of cancer. The 5-Aminolaevulinic acid (ALA) should be one of the most famous hydrophilic non-porphyrinoid PS. Strictly speaking, ALA is not a PS. It is an essential amino acid which plays an important role in the biosynthesis of the heme. The protoporphyrin IX (PpIX), the precursor of heme, is a PS, and injection of excess exogenous ALA could upregulate the accumulation of it in cancer cells. ALA was wildly applied in the treatment of non melanotic skin cancers and cutaneous T-cell lymphoma.

Although the second generation PS made great progress, the development of ideal PS was never stopped.

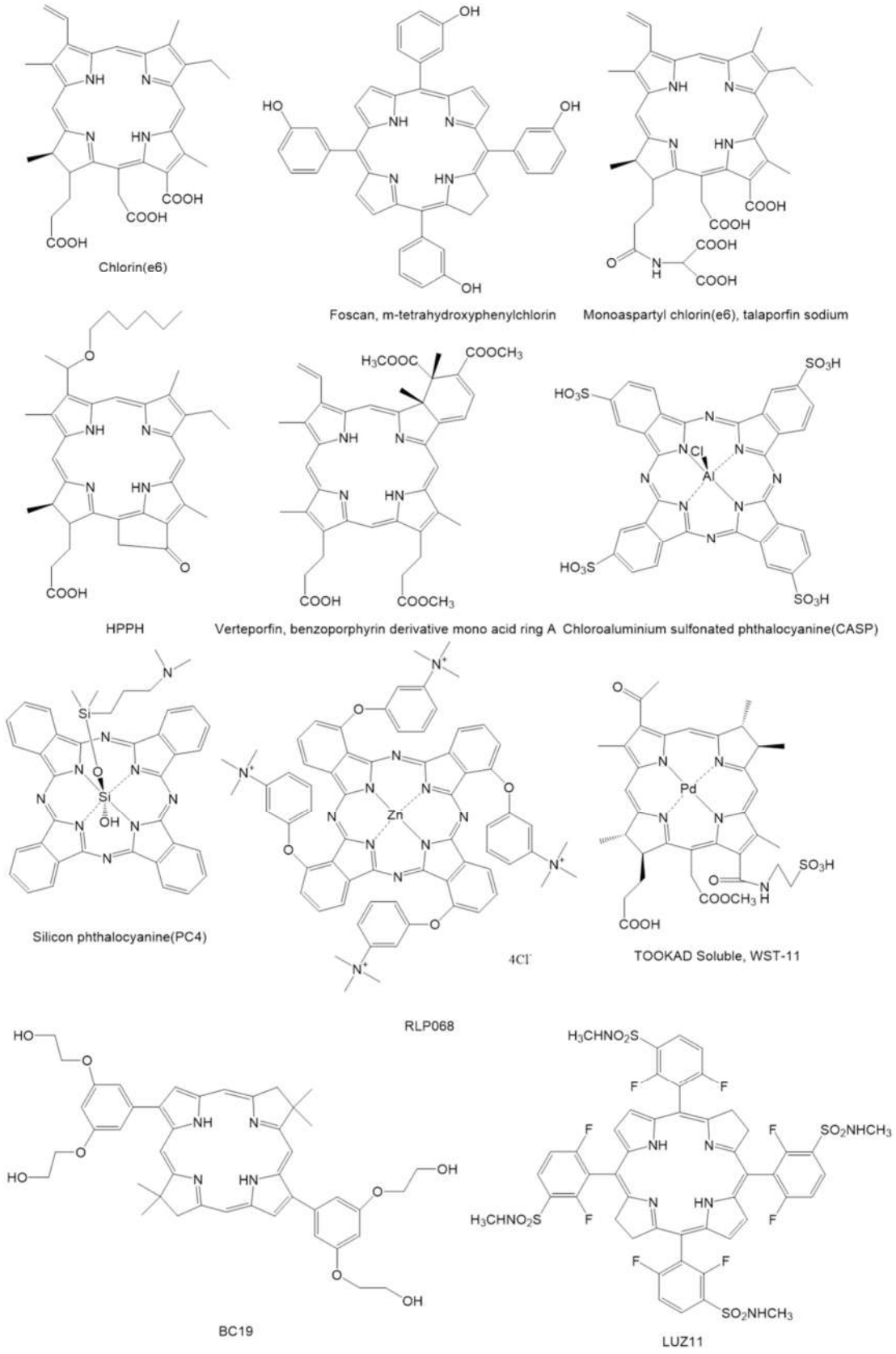

Figure 1.3.2. Structure of several 2nd generation PS.

1.3.3 The third generation PS

Researchers now focus on the development of the next generation PS. The longer wavelength of the activating light, shorter generalized photosensitivity and higher tumor specificity are the critical factors of the new generation PS. The first two factors could be improved by changing the chemical structure of the PS. Indeed, some new PSs which reformed from the second generation PSs already have the improved activating light wavelength and generalized photosensitivity. But the most important factor, tumor specificity, could not be offered to PS by changing the chemical structure. One of the mainstream methods to improve tumor specificity of PSs were modifying the second generation PSs with the biological molecule which has tumor targeting ability, such as antibodies and peptides, to constitute biomolecular-PS conjugates. The other method is constructing delivery systems of PS by conjugating or encapsulating them to vehicles or carriers.

1.4 Current limitations of photodynamic therapy

Nowadays, PDT was used to an independent treatment or an assisted treatment of chemotherapy, radiotherapy, and surgery for cancer. But limited by the delivery and the penetration ability of light, PDT currently was only used in treating the superficial and flat cancers. Although the application of new technology improved the delivery of light, for example, endoscopes, the PDT of bulky tumors or deep-seated tumors was still limited by lack of available techniques and methods to achieve the whole body irradiation. On the other hand, determination of the light dose was also a tricky question in clinical PDT. The insufficient light dose will lead to the incomplete eradication of cancer and relapse which often occurs in the clinic[46]. The excessive light dose will give the damage to the surrounding normal tissue leading to

unfavorable response. Because of the proper PDT light dose depends on the kinds of PSs, there is no widely accepted definition of it. The complexity of the PDT mechanism and lack of suitable clinical measure techniques limited the determination of the light dose. Even the crude relation between the generation rate of $^1O_2$ and light dose could be established by measuring them *in vitro*[47], but light characteristics and the optical tissue properties often made the relationship failed *in vivo*. Researchers now try to develop integrated dosimetry systems and multimodality imaging systems to help clinicians to make customized PDT for patients.

As I introduced in the chapter "Photodynamic Reaction", the oxygen was consumed during PDT treatment. The tumor hypoxia was another limitation of the PDT of cancers. The tumor hypoxia was caused by the rapid growth of cancer and the relatively slow and unprovoked generation of tumor neovascularization. The consumption of oxygen and vasculature damage will exacerbate this phenomenon[48]. The lack of oxygen heavily limited the effect of PDT. Researchers found that splitting the irradiation by dark periods could promote reperfusion of oxygen to compensate for oxygen depletion. And reducing the fluency rate of light was thought to have the same effect. But both of these methods could only relief the hypoxia caused by PDT. The pre-existing hypoxic cells could not be affected by them. Hyperoxygenation therapy was found to compensate for tumor hypoxia in both pre-existing hypoxic cells and those that are acutely induced by PDT. In one study, by hyperoxygenation therapy, the regrowth rate of the tumors was reduced to 20% from 80% (compared with the control group) 60 days after PDT[49]. Oxygen reached critical, chronic hypoxic cells and made them the better response to PDT[50].

Besides the above drawbacks, lack of an ideal PS is still the most significant limitation of clinical utility of PDT, although several first and second generation PSs obtained clinical permission or excellent result in pre-clinical trials. Right now, researchers are doing their best to solve the three most significant problems of PS in the clinical application. The first problem, lack of tumor targeting ability, and the drawbacks caused by it were mentioned above. Some PS preferentially retained in the

tumor cells, rather than the normal cells of the surrounding healthy tissue, but the mechanism of it is not completely cleared. Besides, these tumor accumulations of PSs contributed to the leakage of the vascular system, poor lymphatic drainage, abnormal matrix composition, lower pH, and an increase in the number of low-density lipoprotein receptors,[51] are not enough in most cases. Like other small molecular drugs, PSs should offer the tumor targeting ability by the targeting delivery systems (both of passive and active). The problems caused by unfavorable biodistribution of current PSs, such as prolonged skin photosensitivity and damage to normal tissues should be solved.

Besides the tumor accumulation, the effect of PSs also is affected by the photochemical, photobiological, and pharmacokinetic properties of them. Delocalized aromatic π electron system of the most of PSs gives the ability to absorb light to the PSs, but the structure also made the PSs hydrophobic. The hydrophobicity of PSs leads to poor solubility and aggregation of PSs in aqueous solution, reducing the generation of ROS and finally influencing the effect of PDT. Besides developing water-soluble PS, these problems caused by hydrophobicity could also be solved by a delivery system which keeps the photochemical property of PSs.

1.5 Delivery system of PS

To solve the problem above, the focus of the development of the 3rd generation PS is the study of delivery systems with high specificity to tumor cells or cancer tissues. The conventional method is conjugating the PSs to targeting components, such as peptides, proteins, and antibodies. The nanocarrier without targeting components also was used to deliver the PS by the enhanced permeability and retention effect (EPR)[52,53]. Another benefit of using delivery systems is overcoming the poor water solubility and self-aggregation in aqueous solution without lousy impact to the photochemical of PSs. The nanocarriers used in PDT are including polymeric

nanospheres and nanocapsules, micelles, carbon nanoplatforms, magnetic nanoparticles, and even silica and metal nanoparticles. The improvement of nanotechnology promoted the development of smart nanocarriers and efficient delivery of PS. At the same time, nanocarriers could also prolong the half-life in blood circulation, efficiently control the drug pharmacokinetics and increase bioavailability. However, nanocarriers also have some drawbacks. One of them is the potential problem of tumor tissue penetration of the construct. The large size of the nanocarriers was thought to limit the diffusion of them in the extracellular matrix, leading to accumulation at the periphery of cancer. The inhomogeneous intratumoral distribution should reduce the chance to obliterate cancer. Safety also is an essential problem in the development of nanocarriers of PS. Although lots of nanocarriers were thought to be safe for the patients, the safety of long-team utilization of nanoparticles is not clearly understood. The volume, chemical structure, surface characteristic, hydrophilicity and shape influences the interactions between the nanocarriers and cells/tissues, ultimately decide the safety of the nanocarriers. The most important factor is the components, which determine toxicity and chemical behavior. Biocompatible and biodegradable materials are the first choice for the components of nanocarriers. For the non-biocompatible materials, modification with other biocompatible materials, for example, PEGylation, could improve their safety and keep their additional advantage to a certain degree. Responsive materials also used to compose the nanocarriers. The environmental responsiveness controls the PS release to only targeting tissues after receiving a specific environment signal, such as pH, temperature, light, and ultrasound. As mentioned above, nanocarriers could deliver the PS to cancer by the EPR effect, so-called passive targeting. But they also could be conjugated with a targeting moiety to improve specificity. This active targeting enhances PS bioavailability and is the mainstream in the development of PDT.

Besides being the carriers, some other nanoparticles themselves are the PS, such as fullerenes[54], titanium dioxide[55] and several kinds of quantum dots[56]. Fullerenes could HO• by the Type I mechanism in aqueous environments[57], and the solubility

and biocompatibility could be improved by functionalizing with polar groups as other PSs. Fullerenes have been used to treat mouse colon cancer (CT26), and the survival advantage suggested the potential of fullerenes as PS[58]. Titanium dioxide (TiO2) was well known as a large bandgap semiconductor. The positively charged holes generated during the exciting can produce hydroxyl radicals from the water. Quantum dots were used as the carrier to deliver PSs[59-61] till research showed that quantum dots could act as PS for PDT[56]. After finished the short introduction of nanoparticle PSs, the delivery systems of PS will be introduced in detail in the following chapters.

1.5.1 Organic Nanoparticles

Liposomes

Liposomes may be one of the earliest studied nanoparticles for medicine application, and more than 12 liposomal nanoparticles were allowed to be used in the clinic, and more are in clinical and preclinical trials[62]. Liposomes are concentric phospholipid vesicles consisting of single or multiple bilayered membrane structures. The hydrophilic drugs could be encapsulated in the aqueous core, and the hydrophobic medicines could be encapsulated in their lamellae. This unique characteristic makes them excellent widely used nanocarriers for hydrophilic and/or hydrophobic drugs. Even though, liposomes also have their limitation. Cholesterol is often added to the structure of liposomes to improve the membrane rigidity. However, it will reduce the permeability of encapsulated PS[63]. Liposomes sometimes will exchange the lipid with high-density lipoprotein, leading the decomposition of liposomes and release of PSs[64]. Conventional liposomes also have the short half-life in blood circulation, reducing tumor accumulation[65]. But sufficient sites on the liposomal membrane make it easy to prolong the half-life by conjugating PEG to the liposomes[66]. Besides of PEG, antibodies[67], peptides[68], and glycoprotein[69] also could be readily conjugated to liposomes to synthesize tumor targeting liposomes. Liposomes also have the ability of selective release after modification. These modified liposomes could be sensitive to

pH[70], temperature[71], light[72], and enzymes[73]. The selective release ability could improve the tumor targeting ability of liposome carriers and reduce the side effect of the normal tissues.

Polyester and Polyacrylamide Based Nanoparticles.

Polyester and polyacrylamide are widely used for the formation of micelle and nanoparticle, because of their biocompatibility and biodegradation. Polymeric micelles, polymeric nanosphere, and polymeric nanocapsule are formed to carry hydrophilic or hydrophobic PS by these polymers. Polyester-based PS delivery systems were reported to exhibit great photodynamic efficiency and low photosensitivity[74]. After encapsulation into those nanocarriers, the solubility or dispersion of PSs was improved; leading to improved pharmacokinetic properties. Besides, polymeric nanocarriers deliver the PS to cancer not only by the "passive targeting", but also by the "active targeting", after modified these surfaces with the targeting biomolecules. Therefore, a lot of the second generation PSs were combined with these kinds of polymeric nanocarriers to develop the third generation PSs. Studies on these nanocarriers with different PSs proved that these delivery systems could improve photodynamic activity and anti-tumor effect. On the other hand, the application of them was limited by rapid opsonization and removal from the systemic circulation by the macrophage cells. But this limitation could be broken out by covering the nanocarriers with polyethylene glycol (PEG). PEG-coated nanoparticles shown the enhanced circulation time compared to bare nanoparticles[75,76]. One study illustrated after coated with PEG, the half-life of the nanocarrier increased to 7 hours from around 30 seconds[77]. The biodegradation of the polymer offered one unique advantage of these nanocarriers. Degradation is generally known as a hydrolytic process with or without the enzyme catalyzing effect[78]. After degradation, the polymer will become biocompatible nontoxic products with low molecular weight, and be cleared from the body by physiological pathways and clearance mechanisms.

Premature biodegradation of the polymers generally thought to be the reason for PS leakage, which results in decreased bioavailability. The degradation rate can be controlled by changing the composition, molecular weight of the polymer. Another method to solve this problem is to construct the bioresponsive polymeric systems. For example, one poly-(ethylene glycol) methacrylate-co-2-(diisopropylamino)ethyl methacrylate copolymer based nanoparticles, carrying hydrophobic m-THPC, is very stable in normal body environment (pH=7.4), but unstable in the tumor environment (pH=6.8). This pH-sensitive characteristic could protect the PSs in the blood circulation and enhance the release of PSs in the tumor[79]. Besides these above advantages, the polymeric nanoparticle could become multifunctional delivery systems by packaging diagnostic molecules, the chemotherapeutic agent, and PSs. In conclusion, polymeric nanoparticles are one of the most potential delivery systems.

Dendrimer Based Nanoparticles.

Dendrimers are highly ordered branched molecules, synthesized by a stepwise synthetic procedure. These branched molecules are spherical with the cavity inside in three dimensions. Change the number of synthesis steps could control the size of these molecules. The cavity could be used to carry drugs or other therapeutic molecules. The surface could be modified to adapt for kinds of applications by tagging one or several kinds of targeting molecules and/or functional groups. By changing the size and surface of dendrimers, researchers could improve cellular uptake and tissue biodistribution of PS to achieve better therapeutic effect than free PSs[80]. Two kinds of methods were used to carry PSs by the dendrimers. Like other nanocarriers, the first one is embedding the PS into the dendrimers[81]. However, this method was often limited by the long-termed and complicated preparation and purification. Besides, the low drug loading efficiency is also a problem that cannot be solved easily. The second method is conjugating the PSs to the surface of dendrimers by covalent linkages. These covalent linkages could be broken by the ROS generated by PSs or the cellular

esterases to release the PSs. This method could effectively prevent premature release to increase the accumulation of PSs in target tissues. Moreover, the toxicity of some dendrimers was reduced after being covered by the PSs. However, some researchers worry that the activity of PS might be affected by the new covalent linkages.

1.5.2 Nonbiodegradable Nanoparticles.

Because nonbiodegradable nanoparticles could not release the drugs by degrading themselves, they are not traditionally candidates for drug delivery systems. However, some of them are suitable candidates for PSs delivery systems due to their optical properties and easily controlled shape, size, and porosity. Different from biodegradable nanoparticles, nonbiodegradable nanoparticles release the ROS instead of PSs. Thus, these nanoplatforms can be considered as a modular system that contains thousands of PS molecules, bringing them as a single, nondepleting synergistic unit to the tumor cells.

Silica Nanoparticles.

Silica nanoparticles are widely applied in the PDT due to its chemical stability, transparency to light absorption, structural stability, and great flexibility in synthesis. Moreover, the size, shape, porosity and other characteristics of the silica nanoparticles could be easily changed. Their surface also could be easily modified with kinds of functional moieties or targeting molecules. Similar to dendrimer nanoparticles, the silica nanoparticles could embed the PSs into the silica network or link the PSs by covalent linkages[82]. The first method also may prematurely release the PSs, leading to low treatment efficiency and high side effect. Connecting the PSs in the silica network or the surface could overcome this problem. It was reported that organically modified silica could block the release of loaded PS by the small diameter of pores of it[83]. The

loaded PSs were found to generate ROS efficiently. And the ROS could escape from the carriers freely. Mesoporous silica nanoparticles are another kind of silica nanoparticles with the large surface area and high accessible pore volume. Recently, the mesoporous silica nanoparticles were treated as the base material of multifunctional PS nanocarriers. A nanocarrier composed of a FITC dye-doped silica core and a mesoporous silica shell containing PS was developed to allow imaging and PDT at same time[84]. The covalently linked PSs have shown excellent photo-oxidation efficiency and cell imaging abilities. A phospholipid-capped, protoporphyrin IX-loaded, and FITC-sensitized mesoporous silica nanocarriers were synthesized to deliver PSs to the folic-acid receptor overexpressing tumor cells[85]. This nanoparticle decreased the dark toxicity and increased the cellular uptake of the PS. And the *in vivo* study revealed the nano PDT system mitigated nearly 65% of tumor growth. These studies showed the potential of the application of silica nanoparticles in PDT.

Gold Nanoparticles.

Surface plasmon resonance (SPR) effect and heat conversion ability of gold nanoparticles made them suitable for photothermal therapy (PTT) applications. Hence, the gold nanoparticles carrying PS were used as the agent for photothermal-photodynamic combination therapy. Moreover, localized surface plasmon resonances of gold nanoparticles could increase the excitation efficiency of the accompanying PS. It was reported that after being conjugated with gold nanoparticles, the $^1O_2$ yield of PSs increased 50% in the presence of an associated phase transfer agent (tetraoctylammonium bromide; TOAB), compared with free PSs[86]. In the same work, the gold nanoparticles conjugated PSs gave more damage to endothelial cells, leading to extensive PDT response. However, not only the uptake of gold nanoparticles conjugated PSs in the tumor, but also the uptake in the liver and spleen were enhanced. And the accumulation of these PSs in liver was continued for

seven days. The normal tissues uptake of gold nanoparticles conjugated PSs could be reduced by covering the nanoparticles with PEG[87]. As mentioned above, the wide application of gold nanoparticles in PS delivery systems was due to the potential of photothermal-photodynamic combination therapy. At the early studies of phototherapy-photodynamic combination therapy, two different excitation lights were needed to active PTT and PDT[88]. Recently, both of the therapies could be activated by the same excitation light at the same time after finely designing the structure of the nanoparticles[89,90]. After combined with PDT, the viability of cancer cells was reduced to 11% from 31% (PTT along)[90], demonstrating the anticancer effect of the combinatorial therapy.

Magnetic Nanoparticle

The determining factors of specific PDT design and development were concentrations of the PS in tumor and normal tissues at different time points after injection. But the detection of these data was impossible before the improvement of theranostics nanoprobes. After the establishment of noninvasive, harmless, and visualization technique, magnetic resonance imaging (MRI), researchers have a great method, conjugating PS to MRI contrast agent, to detect the PSs quantitatively *in vivo*. These conjugates were often covered with polymer and/or biomolecules to shield them and achieve active targeting. These multiple functional nanoparticles could achieve excellent cancer targeting delivery, imaging and therapeutic efficiency in vivo at the same time[91-93].

1.5.3 Photosensitizer-antibody conjugates

Monoclonal antibodies (mAb) are potential drugs and ideal carriers for drugs, including PSs, because of the ability to recognize antigens. After conjugation, mAbs

offered the ability to target antigens expressed on tumor cells to PSs, solving the first problem, selective delivery to the cancer cell, in development of the 3rd generation of PSs[94,95]. The first PS-antibody conjugate was synthesized in 1983[96], and it showed better antitumor efficiency compared with the free PSs. With the development of antibody engineering, the PS-antibody conjugate became a promising candidate in the clinic. The immune response made PS-antibody conjugate had the promising application to cancer in the deep site. Hence both of the antibody and PS had the function in therapy, and the conjugation action should not influence the properties of mAb and PS.

1.6 Future directions

Besides PDT, the other functions of PSs, such as “Theranostics”, “Sonodynamic therapy” (SDT), and “Photochemical internalization” (PCI) were developed. Theranostics was the combination of therapy and diagnostics for personally solving the heterogeneous diseases. This technology could optimize the anticancer efficacy, increase comprehensive safety, and promote drug development. Although theranostics has much potential for improving healthcare, a lot of challenges need to be overcome. The most important one is to construct a single platform for diagnosis and therapy at the same time[97]. Besides PDT, PSs are also used as the agent for photodynamic diagnosis (PDD), because of the inherently fluorescent characteristics of PSs[98]. Hence, the PSs were mainly candidates for the theranostics. SDT utilizes ultrasound instead of light to activate some PSs[99]. The most benefit of SDT is to heal the cancers in the deep sites of the body, because of the tissue penetration depth of ultrasound is higher than light. PCI is a technique to enhance the release of together administered drugs via broking the membrane of endosomes by PSs generated ROS. In vitro[99] and in vivo[100] studies proved the effectiveness, and the technology was used to heal head and neck cancer under clinical trials[101]. Not only low molecular agents, but PCI can also

be used for non-viral delivery of nucleic acid-based therapeutics. Delivering nucleic acids (e.g., plasmid DNA, antisense oligonucleotides, siRNA) to target cells could cure many diseases. However, the site of action of nucleic acids requires that these molecules be delivered to the interior of the target cell before being broken by enzymes or other molecules. PCI could enhance the release of nucleic acids from lysosomes or endosomes, which deliver the nucleic acids to the action site and reduce the degradation of the site of action at the same time.

1.7 Significance of This Study

PDT has been receiving greater attention in recent years and has now become an essential field in medical research[102]. But few PSs can be chosen as candidates for clinical application, because most PSs have some drawbacks including hydrophobicity, low photostability, and poor tumor-specificity, which may cause untoward damage to non-cancerous cells and limit the application of PDT[46]. Antibody-PS conjugate was one method to offer the tumor targeting ability to PS. In spite of the outstanding specificity, large size and too strong affinity of antibodies sometimes limit their penetration into deep portions of tumors especially in poorly vascularized tumors, and inhomogeneous antigen expression in a tumor tissue leads to the heterogeneous distribution of the antibodies[103], overshadowing successful PDT.

In this study, to improve the efficacy of PDT, I develop a cRGD functioned polymer conjugate, targeting tumor-associated vasculature of PS to overcome tumor heterogeneity. The cRGD peptide binds explicitly to $\alpha_v\beta_3$ integrin, which is known to be overexpressed on activated endothelial cells of growing vessels and also on melanoma, glioma, lung, ovarian and breast cancer cells[104]. However, the applicability of the monomeric cRGD peptide has been limited by relatively low affinity compared with an antibody and final rapid washout from the tumor. One strategy for overcoming these limitations is the application of multiple cRGD peptides to improve the affinity to the $\alpha_v\beta_3$ integrin[105-108]. But the widely used dendrimer was challenging

to be functioned by more than 4 cRGD peptides, because of difficulty in synthesis or poor hydrophilicity caused by the massive number of cRGD peptides. Therefore, I designed the linear polymer containing 15 cyclic RGD peptides. PS conjugated with the polymer revealed preferential accumulation on the tumor-associated blood vessels without compromising penetration to deep portions of the tumor, thereby drastically inhibiting tumor growth upon photoirradiation, while the polymer containing 5 cyclic RGD peptides showed moderate antitumor activity despite efficient accumulation in the tumor with almost homogenous intratumoral distribution. These results suggest that controlling the intratumoral distribution of IRDye 700DX is critical for successful PDT, and the polymer containing multiple cyclic RGD peptides may be a promising carrier for this spatial control.

Beside of using as agent for PDT, the PS-polymer conjugate also could be used for PCI technology. The low concentration PS-polymer conjugates could massively improve the siRNA transfection. These results revealed that the cRGD peptide functioned polymer could be used as targeting delivery system for several therapeutic agents.

1.8 Outline of the Dissertation

Chapter 2 describes the design, synthesis, and characterization of cRGD peptide functioned polymer and PS-polymer conjugates. Through the ring-opening polymerization method and subsequent deprotection of the side chain, azide functionalized poly(ethylene glycol)-poly(L-glutamic acid) (azide-PEG-PGlu) with narrow molecular weight distribution was first prepared. After activated by the 1,1'-carbonyldiimidazole (CDI), the carboxyl groups were conjugated by the cRGD peptides. The obtained polymers were characterized using ^{1}H NMR and GPC.

Chapter 3 describes the biological activities of the PS-polymer conjugates in *in vitro* and *in vivo* experiment. For investigating the tumor cell targeting ability, cellular uptake efficiency of the PS-polymer conjugates in cell lines overexpressing or down

expressing $\alpha_v\beta_3$ integrin were analyzed by quantitatively measuring the fluorescence intensity via in vivo imaging system (IVIS) and qualitatively observing by confocal microscope. Finally, *in vivo* biodistribution and intratumoral distribution was measured. The high tumor accumulation, tumor-associated vasculature targeting, and homogeneous intratumoral distribution improved the PDT efficacy, proved by the antitumor assay.

Chapter 4 describes the potential of PS-polymer conjugates used as an agent for PCI. The PS-polymer conjugates could improve the siRNA transfection at low concentration.

Chapter 5 describes the summary of the dissertation and future perspectives.

Chapter 2. Synthesis of PS polymer conjugates

2.1 Introduction

The most important section of development of third generation PS is offering the targeting ability to PS by conjugating them to the biomolecules. To improve the PDT efficacy by a, I chosen the integrin $\alpha_v\beta_3$, one of the most promising therapeutic targets for the localization of tumor cells, such as melanoma, glioma, lung, ovarian and breast cancers, and their angiogenesis[109], as the targeting molecule permitting the direct cell death and tumor-associated vasculature damage at same time. Since the cyclic Arg-Gly-Asp (cRGD) peptide specifically binds to the $\alpha_v\beta_3$ integrin, it has been widely used to target $\alpha_v\beta_3$ in vivo. However, monomeric cRGD peptide derivatives sometimes show relatively low tumor accumulation, and rapid tumor washout, limiting their applicability[110]. In this regard, I designed a construct containing multiple cRGD moieties can improve the affinity to the $\alpha_v\beta_3$ integrin, leading to augmented tumor accumulation, and prolonged tumor retention. Many kinds of research have demonstrated that the increase of the number of cRGD peptides in a dendritic structure resulted in improved tumor accumulation and retention, using structures containing two or four cRGD moieties[110]. However, a benefit from the further increased number of cRGD to targeting tumors remains unclear, because the too strong affinity of targeting molecules to the target site sometimes compromises their penetration to the deep region[111]. But conjugating more cRGD peptides in a dendritic structure is limited by the solubility and steric hindrance. In this work, to examine the effect of the number of cRGD peptides on biodistribution and localization in tumor tissue, I have synthesized PS-conjugated polymers containing multiple cRGD peptides (700DX-PEG-PGlu-cRGDx, x=5 or 15) in a linear structure (Figure 2.1.1a), and investigated their distribution in the body and ultimate therapeutic efficacy in in vivo. As a control, a 700DX-polymer conjugate having 15 cyclic RADfK (cRADfK) peptides (700DX-PEG-PGlu-cRAD15), which does not possess affinity to the $\alpha_v\beta_3$ integrin[112], was synthesized similarly, using cRADfK peptides instead of cRGDfK peptides (Figure 2.1.1b). Another control, a monomeric cRGD peptide-functionalized PEG-700DX conjugate (700DX-PEG-cRGD), was synthesized to simulate the

behavior of the monomer cRGD peptide (Figure 2.1.1c).

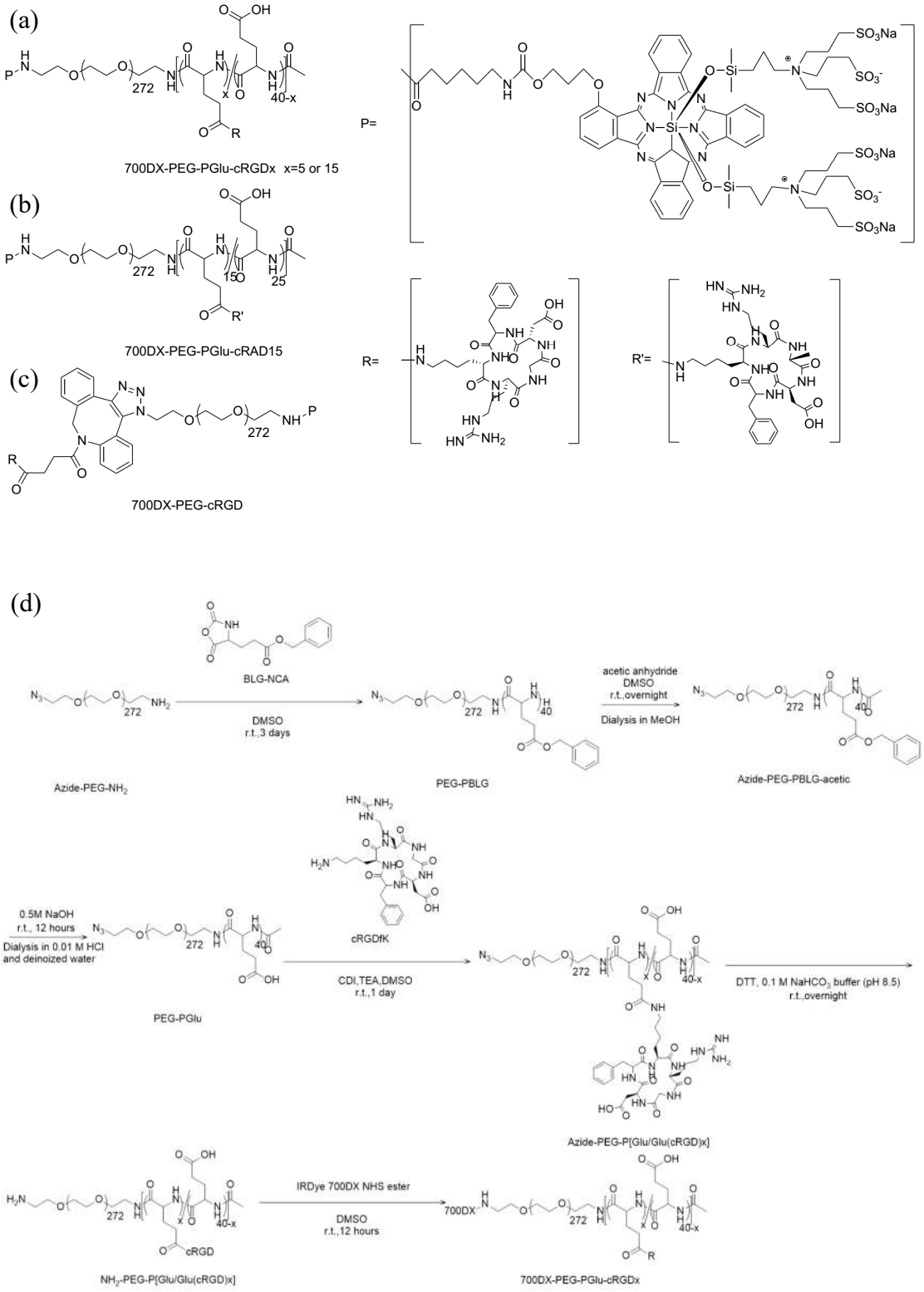

Figure 2.1.1. Schematic diagram illustrating the chemical structure of (a) 700DX-PEG-PGlu-cRGDx, (b) 700DX-PEG-PGlu-cRAD15, and (c)

700DX-PEG-cRGD. (d) Main synthetic scheme of 700DX-PEG-PGlu-cRGDx.

2.2 Materials and Methods

2.2.1 Materials

1,1'-Carbonyldiimidazole (99%) and penicillin-streptomycin were obtained from Sigma-Aldrich Chemical Co. (St. Louis, MO). IRDye® 700DX NHS Ester was obtained from LI-COR, Inc. (Lincoln, NE). Cyclic RGDfK peptide and cyclic RADfK peptide were purchased from Synpeptide (Shanghai, China). γ-Benzyl-L-glutamate *N*-carboxyanhydride was purchased from Chuo Kaseihin Co., Inc. (Tokyo, Japan). Azide functionalized PEG having a terminated hydroxyl group (azide-PEG-OH) was obtained from NOF Corporation (Tokyo, Japan). Dibenzocyclooctyne-N-hydroxysuccinimidyl ester (DBCO-NHS) was purchased from Click Chemistry Tools LLC. (Scottsdale, AZ). Methanesulfonyl chloride (MsCl) and 2,4,6-trinitrobenzenesulfonic acid hydrate (TNBS) were purchased from Tokyo Chemical Industry Co., Ltd. (Tokyo, Japan). Dimethyl sulfoxide (DMSO), *n*-hexane, benzene, triethylamine (TEA), tetrahydrofuran (THF) and sodium hydroxide solution were purchased from Wako Pure Chemical Industries Ltd. (Osaka, Japan). Methanol was purchased from Kanto Chemical Co., Inc. (Tokyo, Japan). DMSO, THF, TEA, and MsCl were distilled over CaH_2 prior to use. Other solvents were directly used without treatment. A series of dialysis membrane with different MWCO were purchased from Spectrum Laboratories, Inc. (Rancho Dominguez, CA) and the centrifugal filter was purchased from Merck Millipore Ltd. (Billerica, MA).

2.2.2 Synthesis of azide-PEG-NH_2

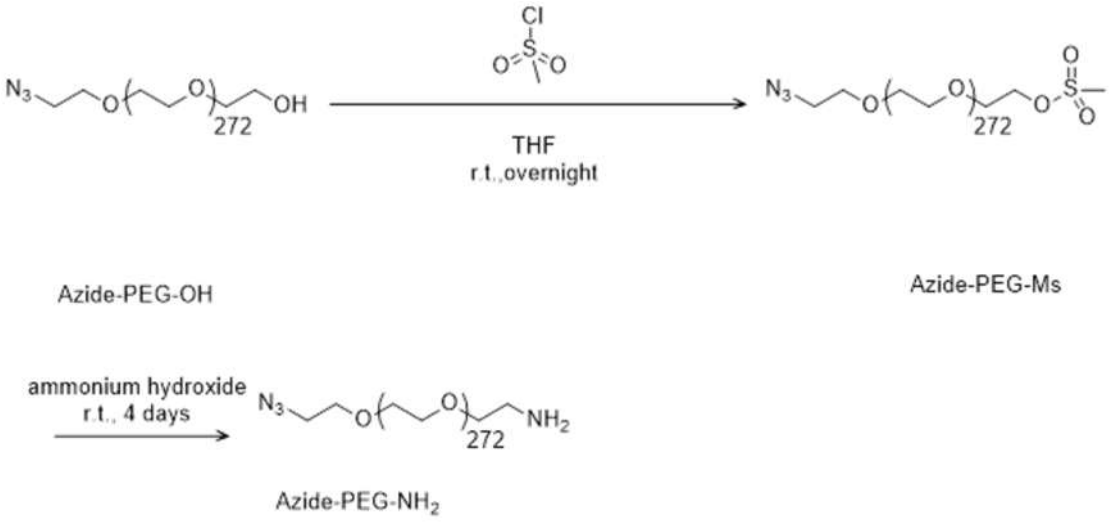

Figure 2.2.1. Synthesis of azide-PEG-NH_2.

To transform the terminative hydroxyl groups of azide-PEG-OH (M_n ~12,000) to an amino group, azide-PEG-OH (2.4 g, 0.2 mmol) was dissolved in 20 mL of benzene, and freeze-dried. The dried azide-PEG-OH was dissolved in 20 mL of anhydrous THF with 150 μL of TEA (1.0 mmol, 5.0 equiv) under argon atmosphere. Four milliliters of THF solution containing 50 μL of MsCl (0.7 mmol, 3.5 equiv) was then added dropwise into the azide-PEG-OH solution. The reaction protected against exposure to light was allowed to proceed at room temperature for 12 h under argon atmosphere. The reaction solution was added dropwise into 700 mL of *n*-hexane to obtain precipitation. The precipitate was collected by vacuum filtration and vacuum drying to produce about 2.1 g of azide-functionalized PEG having a terminated methanesulfonyl group (azide-PEG-mesyl). Azide-PEG-mesyl was then dissolved in 160 mL of aqueous ammonia at the concentration of 25% (w/w). The reaction protected against exposure to light was allowed to proceed at room temperature for four days. After removing the excess ammonia by a rotary evaporator, the solution was dialyzed against deionized water thrice using dialysis membrane (MWCO, 6,000–8,000 Da) at room temperature for 24 h. The crude product was purified by ion exchange column, CX-Sephadex C-50 (Sigma-Aldrich Chemical Co.). The drenched

column was first washed with 0.5% CH_3COOH solution until pH of the solution unchanged after passing the column. Then the acid in the column was washed with deionized water. After the preparation of column, the polymer solution was added dropwise into the column, and then the column was washed with deionized water until the eluent became negative for the indicator for PEG, ammonium thiocyanate solution (0.174 g/ml). Then, 0.125% NH_3, diluted from 25% (w/w) ammonia, was added into the column to elute the azide-PEG-NH_2. After removal of ammonia using a rotary evaporator, the solution was dialyzed against deionized water at room temperature for 12 h using dialysis membrane (MWCO, 6,000–8,000), and the final product was obtained by freeze-drying (1.36 g).

2.2.3 Synthesis of azide-PEG-poly(L-glutamic acid) (PEG-PGlu)

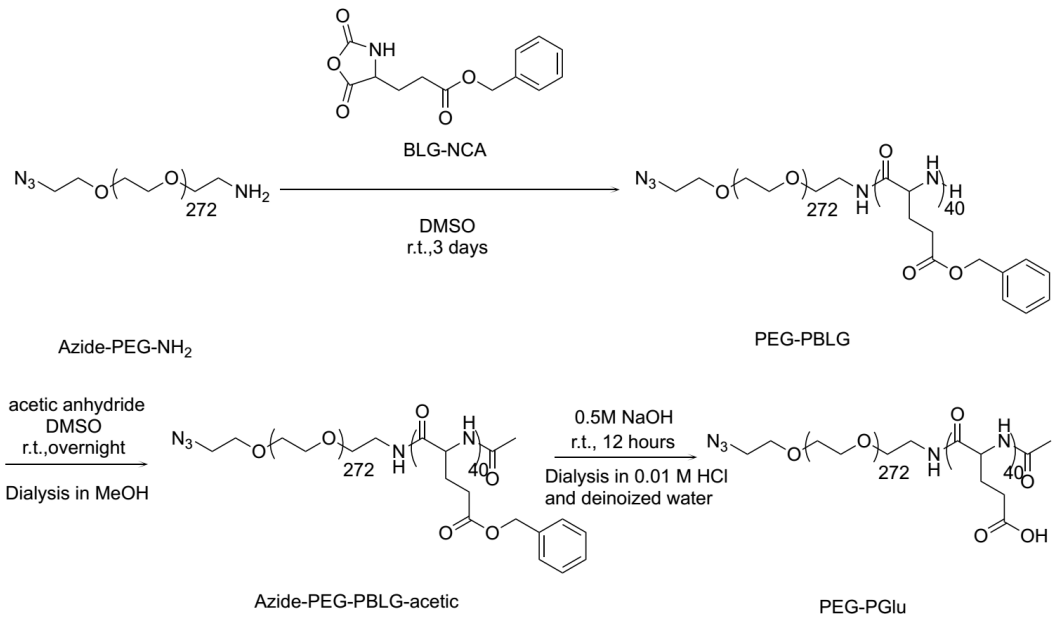

Figure 2.2.2. Synthesis of PEG-poly(L-glutamic acid) (PEG-PGlu).

Azide-PEG-NH_2 (1.2 g, 0.1 mmol) was dissolved in 20 mL of benzene. After freeze-drying, the azide-PEG-NH_2 was dissolved in 20 mL of anhydrous DMSO. Ten milliliters of DMSO solution containing 1.26 g of BLG-NCA (4.8 mmol, 48 equiv)

was added into the PEG solution under argon atmosphere. The reaction was allowed to proceed at 40°C for 3 days under argon atmosphere. The reaction solution was added dropwise into 600 mL of diethyl ether to obtain precipitation of PEG-PBLG. The PEG-PBLG was collected by vacuum-filtration and subsequent vacuum-drying (1.91 g). The polymerization degree of PBLG in PEG-PBLG was determined by ^{1}H NMR. Mw/Mn was determined by GPC [column: TSK-gel superAW3000, superAW4000, and superAWL-guard column (Tosoh Corporation, Yamaguchi, Japan); eluent: NMP containing 50 mM LiBr; flow rate: 0.3 ml/min; detector: refractive index (RI); temperature: 40 °C].

In order to avoid side effects, the ω-end amino group in PEG-PBLG should be acetylated. To achieve the aim, 1.1 g PEG-PBLG was dissolved in 10 mL anhydrous DMSO with excess TEA. After 1 h stirring at room temperature, excess acetic anhydride was added to the solution. After overnight stirring, the solution was dialyzed against methanol twice and deionized water twice with dialysis membrane (MWCO, 12,000–14,000 Da) at room temperature for 24 h. The acetylated PEG-PBLG (azide-PEG-PBLG-acetic) was obtained by freeze-drying (1.02 g).

To deprotect benzyl groups in the PBLG segment of azide-PEG-PBLG-acetic, 1.0 g of azide-PEG-PBLG-acetic was added in 20 mL of 0.5 M NaOH solution. After 12 h stirring, the solution was dialyzed against 0.01 M HCl and deionized water using dialysis membrane (MWCO, 12,000–14,000 Da) at room temperature, followed by freeze dry to obtain 0.85 g of the product.

2.2.4 Synthesis of cRGD-functionalized PEG-PGlu (azide-PEG-P[Glu/Glu(cRGD)]) and cRAD-functionalized PEG-PGlu (azide-PEG-P[Glu/Glu(cRAD)])

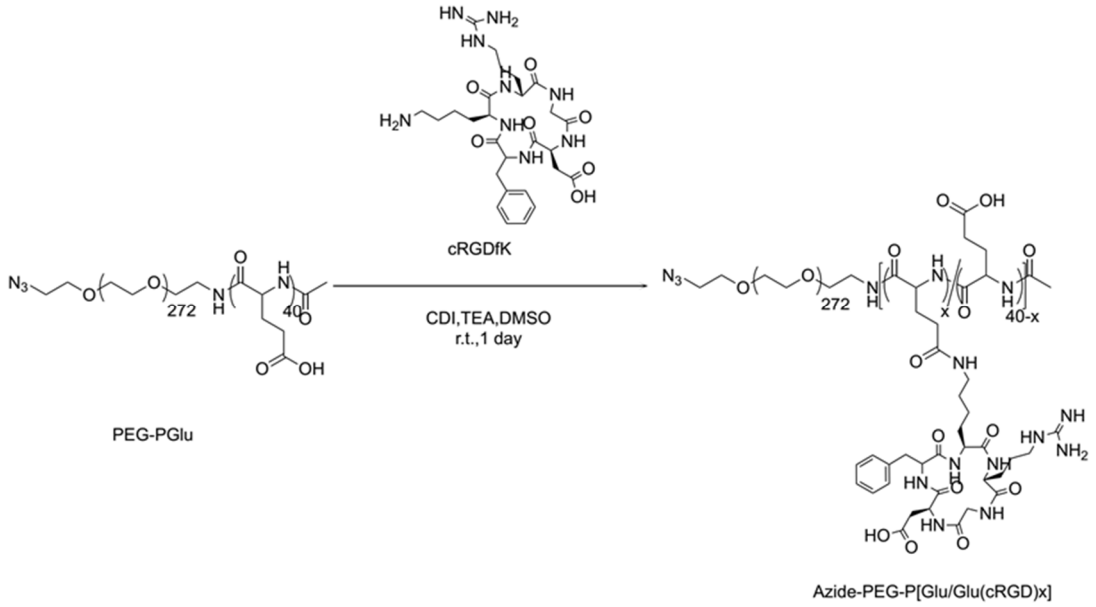

Figure 2.2.3. Synthesis of Azide-PEG-P[Glu/Glu(cRGDx)].

To activate the carboxyl groups of PEG-PGlu, PEG-PGlu (20 mg, 1.17 μmol) and CDI (15.1mg 93.6 μmol) were dissolved in 2 mL of anhydrous DMSO. After 2 h reaction, 2 mL DMSO solution containing cRGDfK (146 mg, 243 μmol) and TEA was added dropwise into the above CDI-activated PEG-PGlu solution. The reaction mixture was stirred at room temperature overnight to produce azide-PEG-P[Glu/Glu(cRGD)]. The mixture was dialyzed against deionized water at room temperature using dialysis membrane (MWCO, 12,000–14,000 Da), and the final product containing 15 cRGDfK peptides, azide-PEG-P[Glu/Glu(cRGD)$_{15}$] was obtained by freeze-drying (24 mg). The other cRGDfK conjugated polymer containing 5 cRGDfK peptides, azide-PEG-P[Glu/Glu(cRGD)$_5$] was produced by changing the ratio of CDI to PEG-PGlu to 40 and rate of cRGDfK to PEG-PGlu to 80.

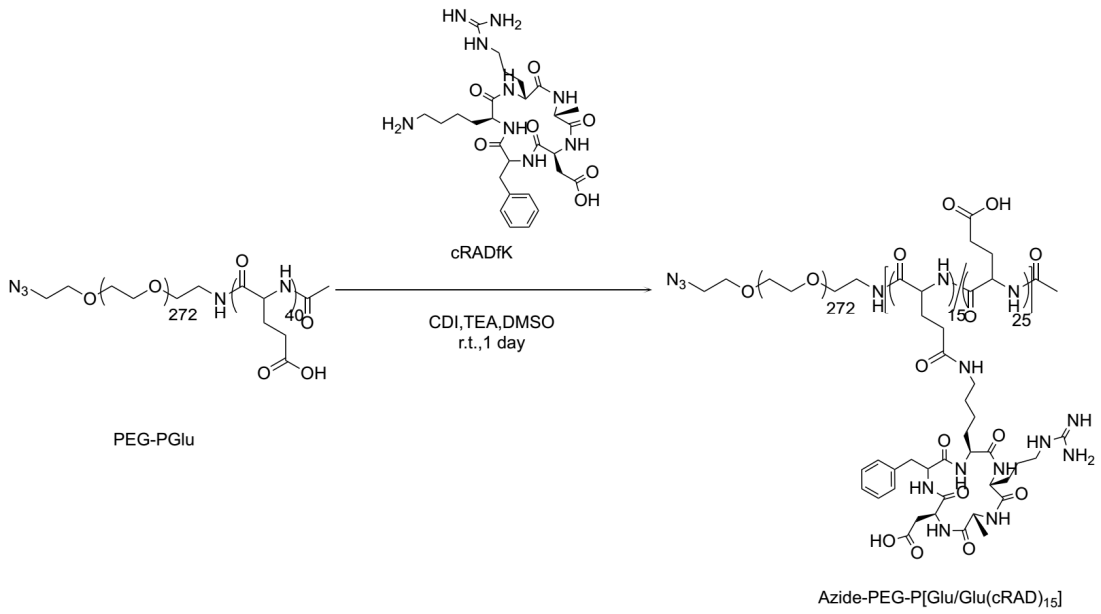

Figure 2.2.4. Synthesis of Azide-PEG-P[Glu/Glu(cRAD)$_{15}$].

Azide-PEG-P[Glu/Glu(cRAD)$_{15}$] was synthesized in the similar method. Then these polymers were purified by HPLC Fraction [column: Superdex200 increased 10/300 GL (GE Healthcare, Chicago, IL); eluent: 10 mM PBS buffer containing 140 mM NaCl; flow rate: 0.5 ml/min]. The number of conjugated cRGDfK peptides or cRADfK peptides was determined by ^{1}H NMR.

2.2.5. Synthesis of 700DX-PEG-PGlu-cRGDx and 700DX-PEG-PGlu-cRAD15

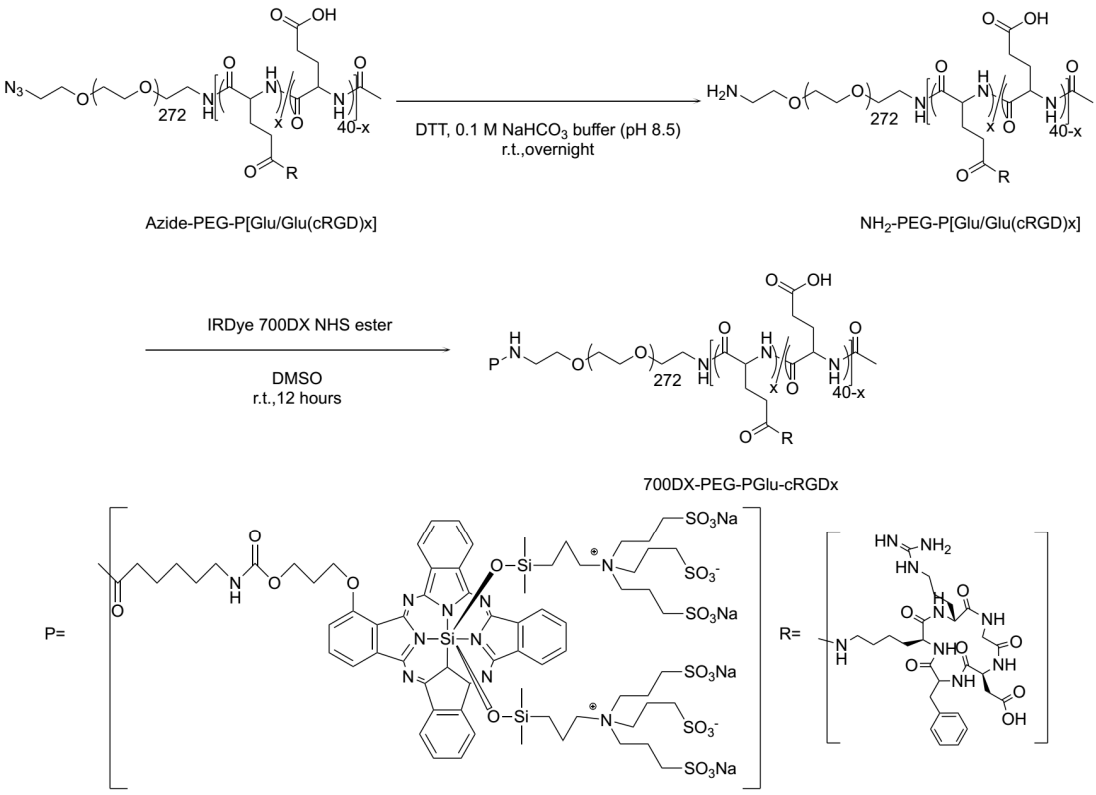

Figure 2.2.5.. Synthesis of 700DX-PEG-PGlu-cRGDx.

To convert the terminal azide group to primary amine group, azide-PEG-P[Glu/Glu(cRGD)] was reacted with DTT (100 equiv) in 2 mL of 0.1 M $NaHCO_3$ buffer (pH 8.5) at room temperature overnight. After dialysis against deionized water and lyophilization, the conversion rate of azide group to amine group was determined to be 90.3% by TNBS Method. The polymer was then dissolved in DMSO, and mixed with DMSO containing 700DX-NHS (1.2 equiv) to conjugate 700 DX to the primary amine group. After dialysis against deionized water at room temperature, the solution was concentrated by a centrifugal filter (MWCO, 10,000), and passed through the Disposable PD-10 Desalting Column (GE Healthcare) to remove unreacted 700DX. The product was obtained by lyophilization and further purified by HPLC. In the procedures as mentioned above in which 700DX was included, the light was avoided as much as possible. The obtained polymer was

characterized by GPC.

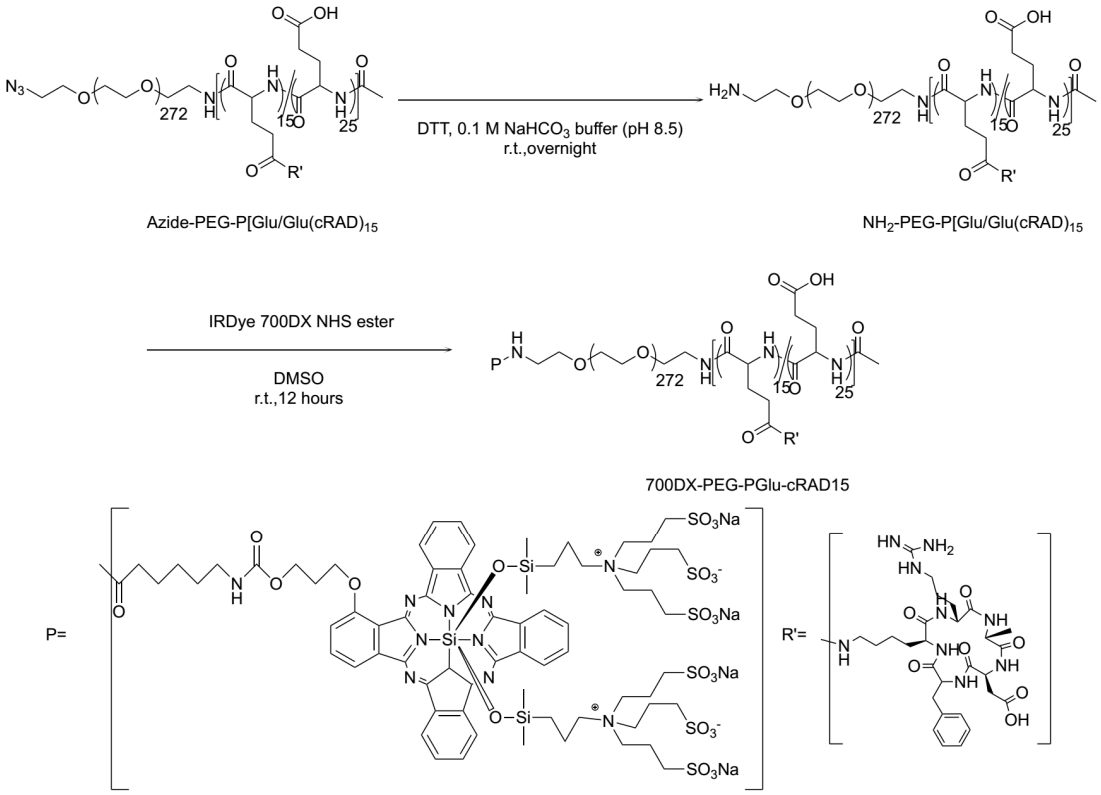

Figure 2.2.6. Synthesis of 700DX-PEG-PGlu-cRAD15.

700DX-PEG-PGlu-cRAD15 was synthesized in the similar method.

2.2.6. Synthesis of 700DX-PEG-cRGD (700DX -PEG-cRGD)

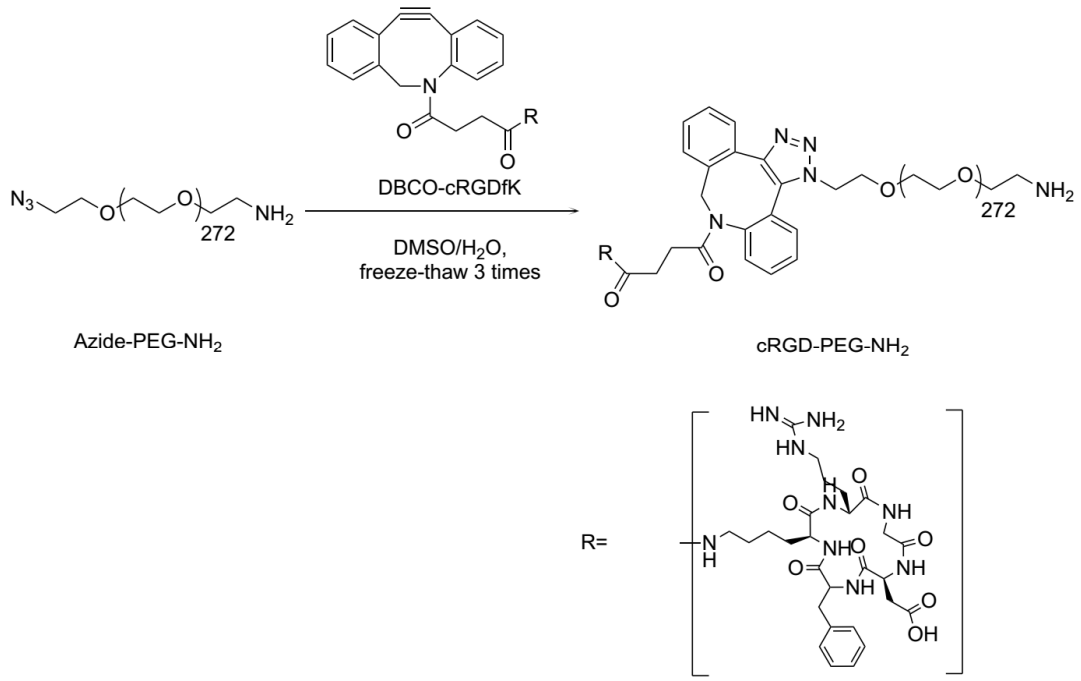

Figure 2.2.7. Synthesis of cRGD-PEG-NH_2.

The cRGDfK peptide (6 mg) was dissolved in 1 mL of DMSO, and mixed with DMSO containing DBCO-NHS (0.2 equiv) to conjugate cRGDfK to the azide group of azide-PEG-NH_2. After 12 h reaction at room temperature, 4 mL deionized water was added into the solution to break unreacted NHS groups. After another 24 h, 12mg of azide-PEG-NH_2 was added into the solution. To promote the click-reaction, the solution was frozen and thawed[113]. After freeze-thawing three times, the solution was dialyzed (MWCO, 6,000–8,000 Da) against deionized water at room temperature. The product was obtained by lyophilization. The introduction of cRGD to polymer was confirmed by ^{1}H NMR.

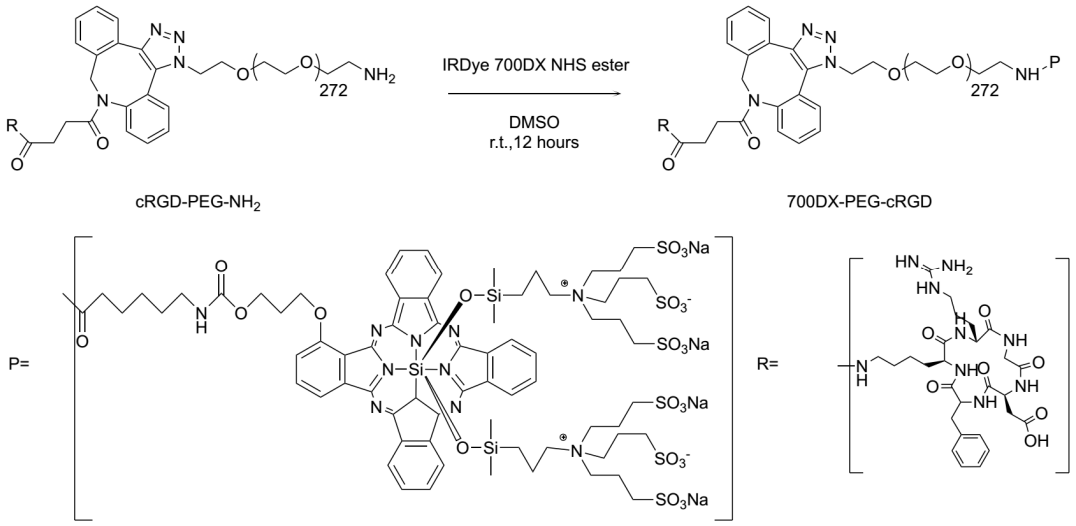

Figure 2.2.8. Synthesis of 700DX-PEG-cRGD.

The obtained polymer was dissolved in DMSO, and mixed with DMSO containing 700DX-NHS (1.2 equiv) to conjugate 700 DX to the amine group. After dialysis (MWCO, 6000 ~ 8000 Da) in deionized water 3 times, the solution was concentrated by a centrifugal filter (MWCO, 10,000) and passed through the Disposable PD-10 Desalting Column to purify the polymer. In the aforementioned procedures in which 700DX was included, light was avoided as much as possible. The product was obtained by lyophilization and further purified by HPLC.

2.3 Results and Discussion

To synthesize the linear skeleton of the PS polymer conjugates , azide-PEG-PBLG was synthesized in accordance with Figure 2.2.2. According to the Figure 2.3.1, the initiator, azide-PEG-NH_2, was successfully synthesized and purified by the method shown in Figure 2.2.1.

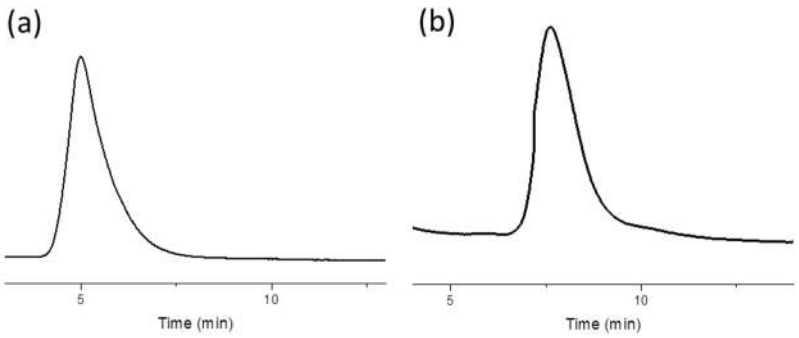

Figure 2.3.1 GPC result of (a) azide-PEG-OH and (b) azide-PEG-NH_2. Column: SQ-5wp (GE Healthcare Life Sciences, Marlborough, MA); eluent: 10 mM PBS buffer containing 140 mM NaCl; flow rate: 0.5 ml/min, detector: ultraviolet (UV, wavelength: 220nm)].

Then, polymerization of BLG-NCA was initiated by azide-PEG-NH_2 to afford PEG-PBLG. The polymerization degree of PBLG in PEG-PBLG was determined to be 40 by ^1H NMR (Figure 2.3.2.) and Mw/Mn was determined to be 1.10 by GPC (Figure 2.3.3.).

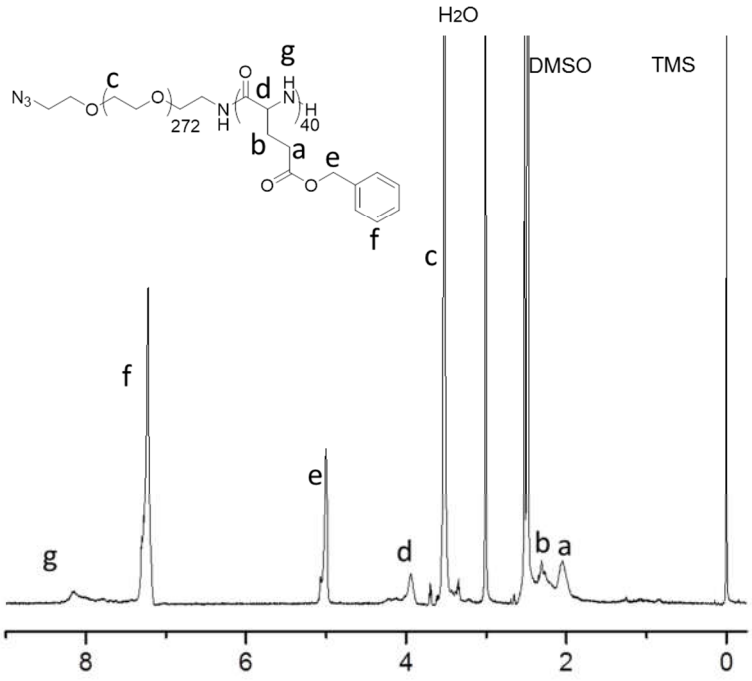

Figure 2.3.2. ^{1}H NMR spectrum of azide-PEG-PBLG (DMSO-d_6, 80°C).

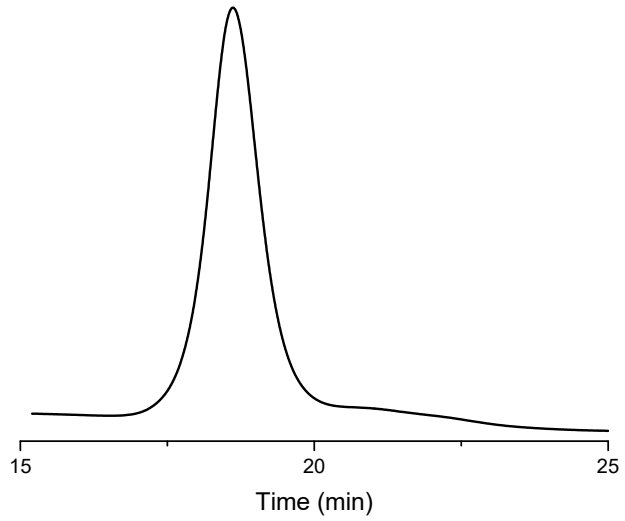

Figure 2.3.3. GPC result of PEG-PBLG. [Column: TSK-gel superAW3000, superAW4000, and superAWL-guard column (Tosoh Corporation, Yamaguchi, Japan); eluent: NMP containing 50 mM LiBr; flow rate: 0.3 ml/min; detector:

refractive index (RI); temperature: 40 °C].

Benzyl groups were deprotected, and the successful deprotection was proved the disappearance of the peak of proton of benzyl groups in ^{1}H NMR (Figure 2.3.4.). And the PDI (1.11) was constant after deprotection (Figure 2.3.5.).

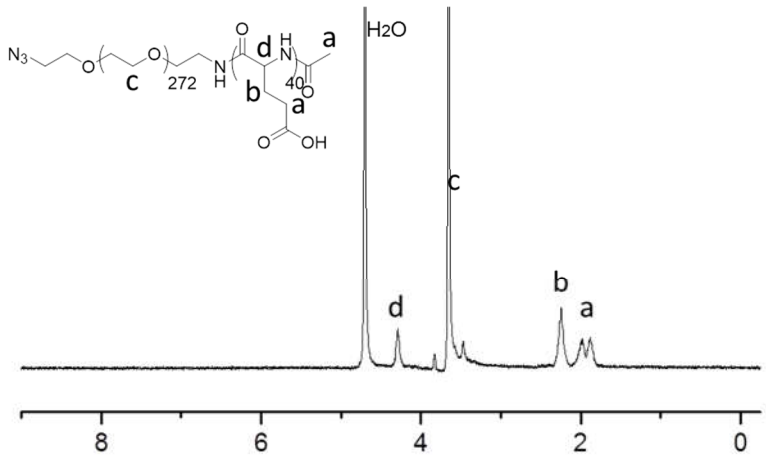

Figure 2.3.4. ^{1}H NMR spectrum of azide-PEG-PGlu (D_2O, 25°C).

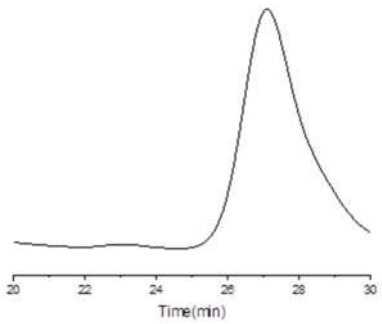

Figure 2.3.5. GPC results of PEG-PGlu. [Column: Superdex 200 increase 10/300 GL (GE Healthcare Life Sciences, Marlborough, MA); eluent: 10 mM PBS buffer containing 140 mM NaCl; flow rate: 0.5 ml/min, detector: ultraviolet (UV, wavelength: 220nm)].

The number of conjugated cRGD peptides and cRAD peptides was determined to be 1,

5, 15 and 15 by ^{1}H NMR (Figure 2.3.6-9).

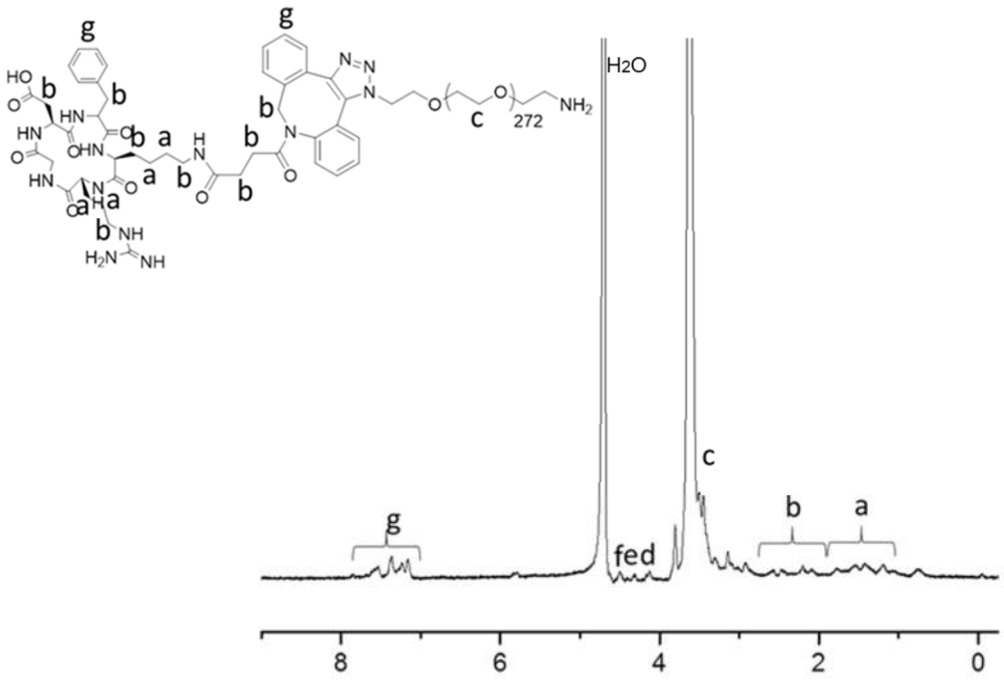

Figure 2.3.6. ^{1}H NMR spectrum of cRGD-PEG-NH_2 (D_2O, 25°C).

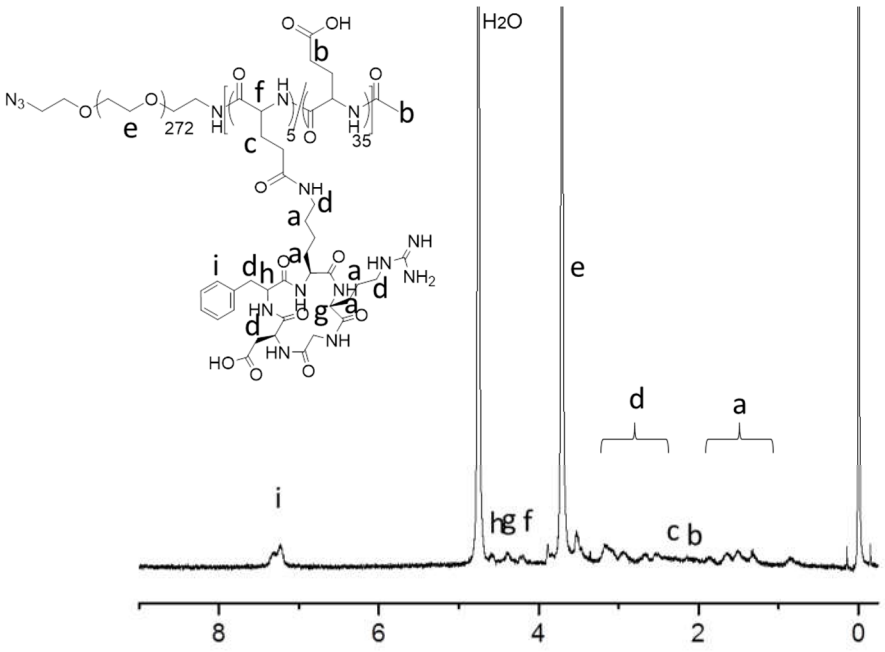

Figure 2.3.7. ^{1}H NMR spectrum of azide-PEG-PGlu-cRGD5 (D_2O, 25°C).

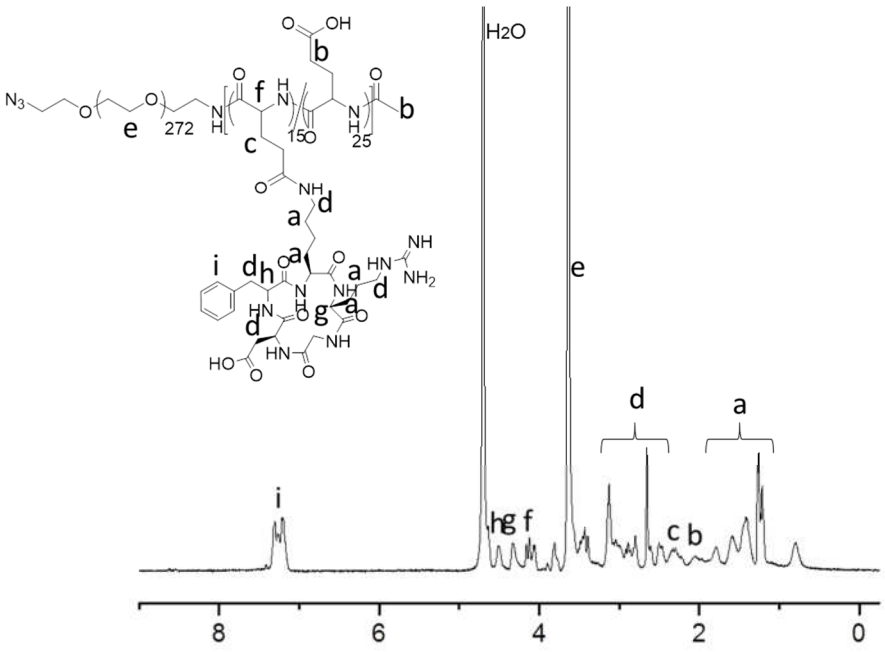

Figure 2.3.8. ^{1}H NMR spectrum of azide-PEG-PGlu-cRGD15 (D_2O, 25°C).

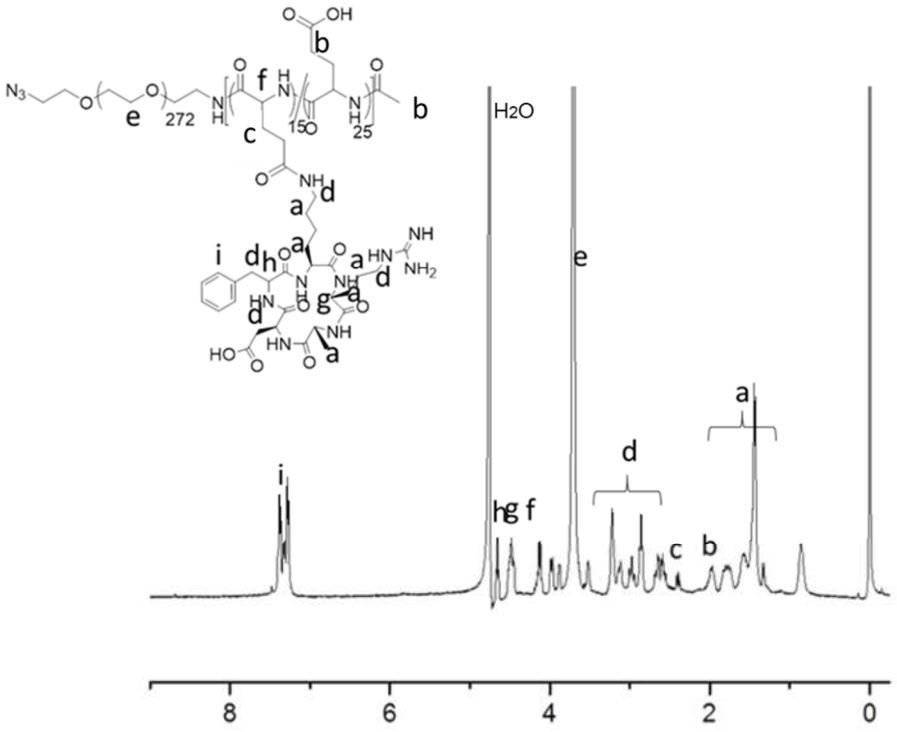

Figure 2.3.9. ^{1}H NMR spectrum of azide-PEG-PGlu-cRAD15 (D_2O, 25°C).

Finally, PS-NHS was conjugated to amine group at the polymer terminus. All of the obtained polymers showed monodispersed molecular weight distribution (Figure 2.3.10), indicating the structure of these polymers was not destroyed after the introduction of PS. And the different time point of the appearance of the peaks also proved the conjugate of peptides.

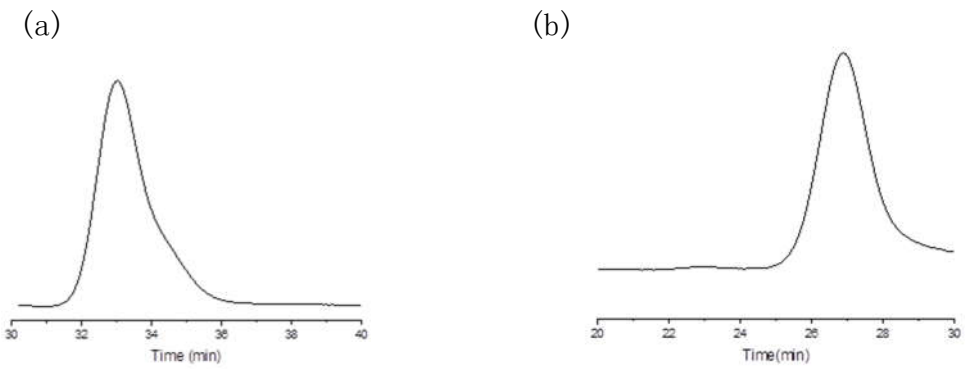

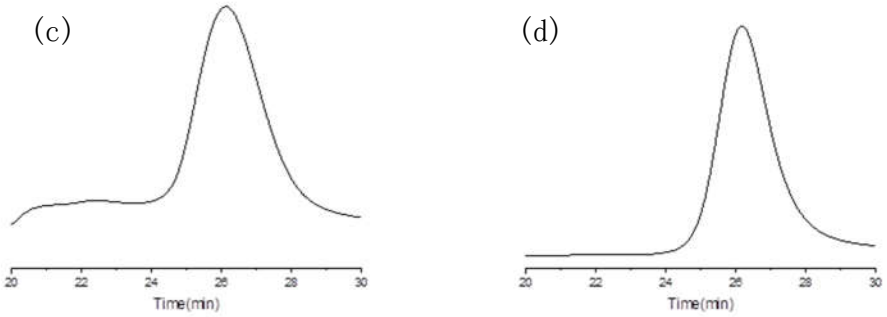

Figure 2.3.10. GPC results of (a) 700DX-PEG-cRGD, (b) 700DX-PEG-PGlu-cRGD5, (c) 700DX-PEG-PGlu-cRGD15, and (d) 700DX-PEG-PGlu-cRAD15. [Column: Superdex 200 increase 10/300 GL (GE Healthcare Life Sciences, Marlborough, MA); eluent: 10 mM PBS buffer containing 140 mM NaCl; flow rate: 0.5 ml/min, detector: ultraviolet (UV, wavelength: 220nm)].

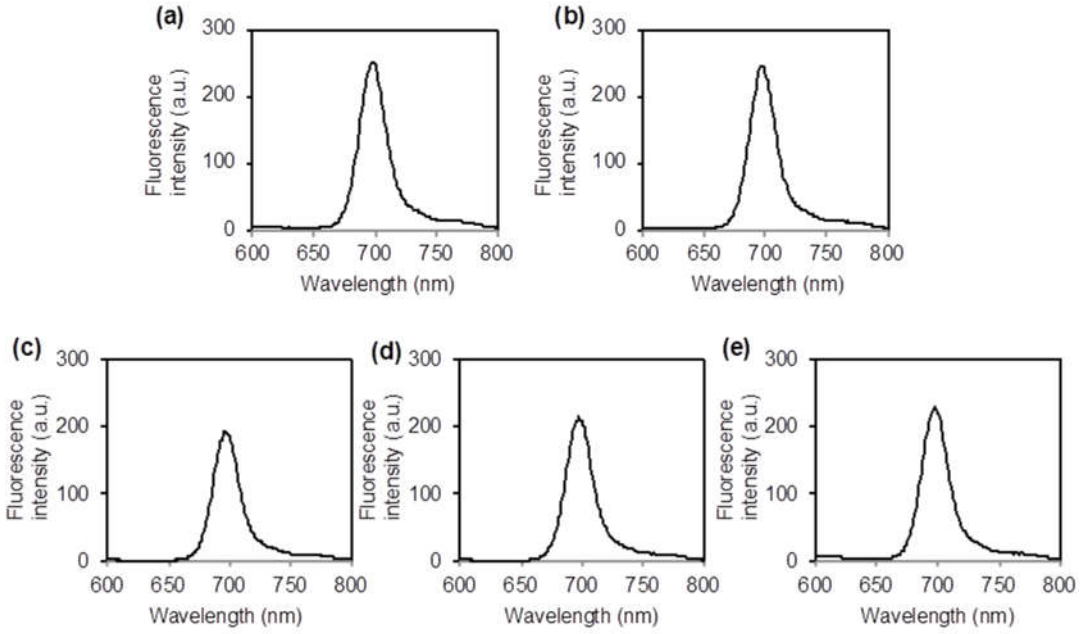

Figure 2.3.11. Fluorescence spectra of (a) 700DX, (b) 700DX-PEG-cRGD, (c) 700DX-PEG-PGlu-cRGD5, (d) 700DX-PEG-PGlu-cRGD15, and (e) 700DX-PEG-PGlu-cRAD15 (excitation wavelength: 550 nm).

Also, I measured fluorescence spectra of the synthesized 700DX-conjugated polymers

(Figure 2.3.11) by a fluorophotometer (FP-8300, JASCO Corporation, Tokyo, Japan, the excitation wavelength was 550 nm). All the polymers emitted the similar fluorescence with 700DX, suggesting that the conjugation of 700DX to the polymers did not affect its photoactivity.

In this study, the linear construct containing multiple cRGD moieties was synthesized. Poethko et al. reported for the simultaneous binding of two peptide motifs to the receptors, the distance between two RGD motifs should be more than 3.5 nm (~25 bond distances). The structure of PGlu is conducive to ensure the average distance between two RGD motifs more than 25 bond distances, assuming the peptides conjugated to the polymer evenly. At the same time, the PGlu could avoid the dissolving problems happened to the dendritic structure containing about 16 cRGD peptides. The PEG was also contributed to the hydrophilicity, and it enhanced the stability of the conjugates by covering the PS during the blood circulation. And the relatively small size of the structure, compared with other kinds of PS delivery systems, promoted the clearance of PS and tumor penetration.

In conclusion, the PS-polymer conjugates were successfully synthesized by ring-opening polymerization of BLG-NCA and subsequent side chain modification. All polymers showed narrow molecular weight distribution after conjugated with peptides and PSs, proving the stability of the polymer structure. The photostability of PS also stays at a similar level after the conjugation reaction.

3. Biological activities of PS-polymer conjugates

3.1 Introduction

Integrin $\alpha_v\beta_3$ is overexpressed on activated endothelial cells of growing vessels and also on a lot of tumor cells. Hence, it has been one of the most promising therapeutic targets for the localization of tumor cells and their angiogenesis.[1] The cRGD peptide, with the specifical binding ability to the $\alpha_v\beta_3$ integrin, has been widely used in vivo. However, the application of monomeric cRGD peptide was limited by low tumor accumulation, and rapid tumor washout.[2] In this regard, I synthesized a construct containing multiple cRGD moieties, as described in chapter 2, to improve the affinity to the $\alpha_v\beta_3$ integrin, leading to augmented tumor accumulation, and prolonged tumor retention.

In this chapter, I will discuss the biological interaction between PS-polymer conjugates and tumor cells in *in vitro* and *in vivo*. By determining the fluorescence intensity via IVIS, the enhanced interaction between the PS-polymer conjugates and the cells potentially improves the cellular uptake efficiency of the PS. And this phenomenon was not found in the integrin downregulated cell line. Beside of this experiment, confocal laser scanning microscopic observation was also performed to confirm the cell uptake and examine internalized pathway. Compared with the cell uptake results, the increased phototoxicity could only be found in the integrin upregulation cell line. Finally, to assess the in vivo biodistribution, intratumoral distribution and antitumor efficacy, PS-polymers polymer were intravenously injected into the mice. Their retention at the tumor site was evaluated by IVIS and homogenized tissue solution. Their intratumoral distribution was tested by the confocal laser scanning microscopic observation of tumor tissue directly. Their antitumor efficacy was assessed by measuring tumor size after photoirradiation.

3.2 Materials and Methods

3.2.1 Materials

Lysotracker Red DND-99 and Hoechst33342 were obtained from Thermo Fisher Scientific, Inc. (Waltham, MA). Dulbecco's modified Eagle's medium (DMEM), penicillin/streptomycin, and trypsin/EDTA were purchased from Sigma Aldrich Corporation. D-PBS(-) (PBS) were purchased from Wako Pure Chemical Industries, Ltd. Passive Lysis Buffer was purchased from Promega Corporation, (Madison, WI).

3.2.2 Cell Culture

U87MG and K562 cell lines were purchased from American Type Culture Collection (ATCC) (Manassas, VA). U87MG cells were grown in Eagle's minimum essential medium containing 10% fetal bovine serum and 1% penicillin and streptomycin. The medium for K562 was Iscove's modified Dulbecco's medium containing 10% FBS and 1% penicillin and streptomycin. Cells were incubated at 37°C in a humidified atmosphere containing 5% CO_2.

3.2.3 Cellular uptake

Cells were seeded in a 96-well plate (Greiner Bio-One GmbH, (Frickenhausen, Germany)) at a density of 1 x 10^4 cells/well for 24 h. The culture medium was replaced with fresh medium containing the polymers at various concentrations in the absence or presence of free cRGDfK peptides. After 7 h incubation and medium replacement, the cells were lysed by 100 μL of Passive Lysis Buffer. After 30 min incubation, 50 μL of lysate from each well was transferred to black 96 well plates (Thermo Fisher Scientific, Inc. (Waltham, MA)), and the fluorescence of 700DX was quantified by *in vivo* imaging system (IVIS, Perkin Elmer, Waltham, MA) (ex/em = 710 nm/780 nm). For each sample, the average fluorescence was calculated from 6

wells.

3.2.4 Confocal laser scanning microscopic observation of subcellular distribution

U87MG cells were seeded at the density of 1 x 10^5 cells/dish in 35-mm glass-based dishes. After 24 h incubation, cells were incubated in fresh medium containing various concentrations of PSs for 7 h. To stain lysosomes, Lysotracker Red DND-99 was added into each well at a concentration of 50 nM 30 min before the end of incubation. Cells were then washed three times by 1 ml of PBS and fixed by PBS containing 4% paraformaldehyde and Hoechst33342 (10 μg/mL) to stain cell nuclei. Cells were washed with PBS three times and then observed in PBS using a confocal laser scanning microscope (LSM710, Carl Zeiss AG, Oberkochen, Germany).

3.2.5 Cell viability

The cytotoxicity was evaluated using the Cell Counting Kit 8 assay in U87MG cells and K562 cells. U87MG Cells were seeded in a 96-well plate at a density of 1 x 10^4 cells/well for 24 h. For K562 cells, a U-shape 96-well plate (Greiner Bio-One GmbH) was used. The culture medium was replaced with fresh medium containing the PSs at various concentrations. After 7 h incubation and medium replacement, the cells were photoirradiated using a halogen lamp equipped with a band filter (400–700 nm) at fluence of 3.0 mW/cm^2 for 1 h in fresh medium on ice, followed by additional incubation for 48 h. After replacing the old medium, 100 μL of medium containing 10 μL of Cell Counting Kit 8 solution was added to each well and cells were incubated for 2 h. The absorbance at a wavelength of 450 nm was measured using iMark Microplate Reader (BIO-RAD (Hercules, CA)). The cell viability was calculated from the following equation:

Cell viability (%) = ([A]test – [A]blank) / ([A]control – [A]blank) × 100,

where [A]test, [A]control and [A]blank are the absorbance values of the cells treated

with the samples, non-treated cells, and medium without cells, respectively. For each sample, the average absorbance was calculated from 6 wells.

3.2.6 Biodistribution study

Four-week-old female BALB/c nude mice were obtained from Charles River Laboratories Japan, Inc. (Yokohama, Japan). To make a subcutaneous tumor model, 1 x 10^6 U87MG cells were injected subcutaneously in the left dorsum of each mouse. When the tumor volume reached approximately 400 mm^3, PSs were intravenously injected to the mice (10 μg of 700DX/mouse), and fluorescence of 700DX in the body was imaged at indicated time points using IVIS (ex/em = 710 nm/780 nm). Also, to quantify the accumulated amount of 700DX, tumors and organs were taken out from the mice and gently washed by PBS at indicated time points. After removing the excess fluid by tissue paper, the tumors and organs were mixed with Passive Lysis Buffer, and homogenized by a Handy Sonic (TOMY SEIKO Co., Ltd., Tokyo, Japan). The homogenized solutions were transferred to black 96 well plates, and the fluorescence of 700DX was quantified using IVIS (ex/em = 710 nm/780 nm).

3.2.7 Microscopic observation of intratumoral distribution

To observe the intratumoral distribution of the PSs in tumor tissue, subcutaneous tumor models were prepared in the same way with the biodistribution study. When the tumor volume reached about 200 mm^3, mice were injected with samples (10 μg of 700DX/mouse). Two and half hours after intravenous injection of the samples, the mice were additionally injected with 100 μL of PBS buffer containing 250 μg of Hoechst33342 and 25 μg of Lycopersicon esculentum lectin, DyLight 488 Conjugate (Vector Laboratories,(Burlingame, CA)) to stain nuclei and blood vessels, respectively. The tumor was then gently taken out and cut in half after sacrificing the mice. The tumor was directly observed by an LSM710 confocal laser scanning microscope, immediately after collecting the tumor.

3.2.8 In vivo antitumor activity

To determine tumor volume, long axis (length) and short axis (width) from each tumor were measured using a caliper. Each tumor volume was calculated using the following equation:

tumor volume = length × width^2 × 0.5.

Subcutaneous tumor models were prepared in the same way with the biodistribution study. Animals were randomized into 6 groups (6 mice/group): (1) no treatment, (2) 700DX, (3) 700DX-PEG-cRGD, (4) 700DX-PEG-PGlu-cRGD5, (5) 700DX-PEG-PGlu-cRGD15, and (6) 700DX-PEG-PGlu-cRAD15. When tumor volume reached approximately 15 mm^3, the samples (30 μg of 700DX/mouse) were intravenously injected to the mice through tail veins. Three hours after intravenous injection, tumors were photoirradiated using a diode laser (680 nm) at fluence of 100 mW/cm^2 for 1,000 s. Tumor volume was measured every three days until it reached 2,000 mm^3.

3.3 Results and Discussion

3.3.1 Cellular uptake and subcellular distribution

The *in vitro* cellular uptake of the PSs was assessed by measuring the fluorescence intensity of PSs in U87MG (human glioblastoma) cells overexpressing $\alpha_v\beta_3$ integrin and K562 (human myelogenous leukemia) cells with the low expression level of $\alpha_v\beta_3$ integrin[114], using flow cytometry. Figure 3.3.1a shows cellular uptake of PSs at various concentrations in U87MG cells. The 700DX-PEG-cRGD, 700DX-PEG-PGlu-cRGD5, and 700DX-PEG-PGlu-cRGD15 revealed significantly high cellular uptake depending on the number of cRGD peptides, while no significant difference could be obtained between free 700DX and 700DX-PEG-PGlu-cRAD15. Especially at 700DX concentration of 200nM, the fluorescence intensity of the cells

treated by 700DX-PEG-PGlu-cRGD15 was 4.5 times and 2.5 times higher than that of cells incubated with free 700DX and 700DX-PEG-cRGD, respectively. In contrast, as shown in Figure 3.3.1b, 700DX-PEG-cRGD, 700DX-PEG-PGlu-cRGD5, and 700DX-PEG-PGlu-cRGD15 did not show the drastic increase of cellular uptake in K562 cells. These results suggest the specificity of cRGD to $\alpha_v\beta_3$ integrin and improved uptake by increasing the number of conjugated cRGD peptides. Note that free 700DX did not show concentration-dependent cellular uptake in both U87MG and K562 cells. Such low cellular uptake of 700DX was also reported in a different cell line in a previous study[115], which is an inherent property of 700DX. To gain more insight about the specificity of 700DX-PEG-cRGD, 700DX-PEG-PGlu-cRGD5, and 700DX-PEG-PGlu-cRGD15 to $\alpha_v\beta_3$ integrin, I also examined their cellular uptake in U87MG cells in the presence of excess free cRGDfK peptides (Figure 3.3.1c). The excess free cRGDfK peptides markedly inhibited the cellular uptake of the polymers containing cRGD peptides, and the higher concentration of free cRGDfK peptides more efficiently lowered the cellular uptake, while 700DX and 700DX-PEG-PGlu-cRAD15 did not show the inhibited cellular uptake. Taken together, 700DX-PEG-cRGD, 700DX-PEG-PGlu-cRGD5, and 700DX-PEG-PGlu-cRGD15 should possess the selective affinity to $\alpha_v\beta_3$ integrin.

To examine subcellular distribution of the PSs, I observed the U87MG cells incubated with the PSs, using confocal laser scanning microscopy (CLSM) (Figure 3.3.1d). Consistent with the cellular uptake shown in Figure 3.3.1a, 700DX-PEG-cRGD, 700DX-PEG-PGlu-cRGD5, and 700DX-PEG-PGlu-cRGD15 revealed considerably high fluorescence intensity of 700DX in the cells compared to free 700DX. Irrespective of cellular uptake efficiency, all the PSs were colocalized with Lysotracker Red DND-99 that stains acidic organelles including lysosomes, suggesting that the PSs were internalized into the cells via an endocytic process.

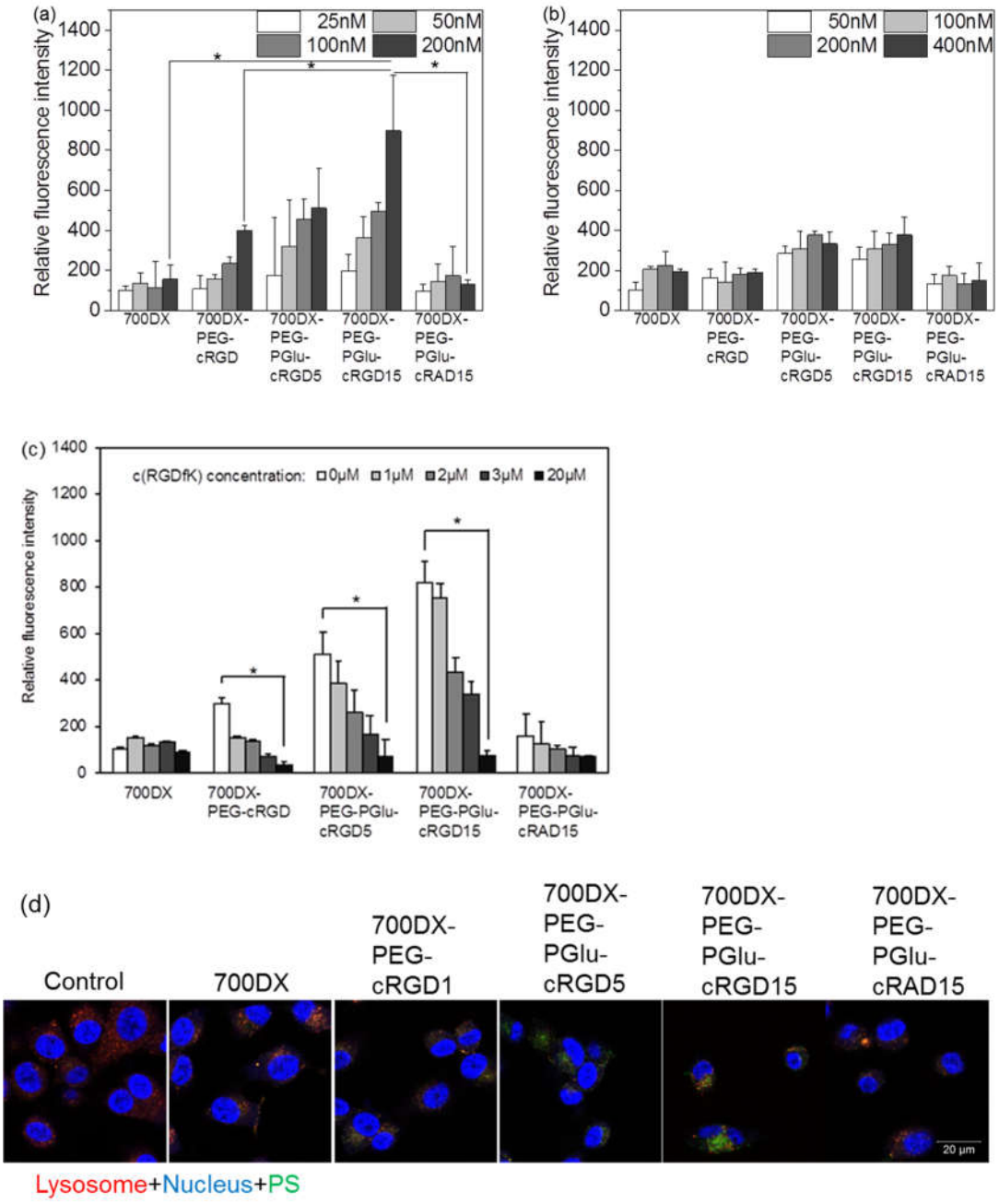

Figure 3.3.1. (a–c) Cellular uptake study. Cellular uptake was evaluated by measuring fluorescence intensity of PSs in (a) U87MG, (b) K562 cells, and (c) U87MG cells with exceed free cRGD peptides. (d) Subcellular distribution of PSs in U87MG cells.

Since travel distance of singlet oxygen that is considered to be the most cytotoxic ROS in PDT is several ten nanometers in cells[116], the therapeutic outcome of PDT is governed by selective accumulation of PS in malignant cells. However, the antitumor efficacy of PS delivery systems is sometimes compromised by their limited

penetration from perivascular regions to the deep parts of the tumor, caused by too strong affinity. For example, previous studies reported that limited penetration of antibodies should be due to too strong binding of antibodies to cells peripheral to blood vessels, which phenomenon is so-called a binding site barrier[117]. Thus, the fine-tuning affinity of delivery systems is important to control intratumoral distribution. In this context, I have utilized PEG-PGlu as a platform to mount 700DX and multiple cRGD peptides whose affinity could be controlled by changing the number of cRGDs. The increase in the number of cRGD peptides has been reported to permit multivalent binding, constant rebinding owing to the high local concentration of the peptide, and integrin clustering initiated by cRGD binding to the cell surface, thereby augmenting affinity, cellular uptake, tumor specificity, and tumor retention[118]. The increased cellular uptake and tumor accumulation were indeed obtained in many tetrameric cRGD peptides conjugate systems[106,108,119]. 700DX-PEG-PGlu-cRGD5 also exhibited the improved cellular uptake (Figure 3.3.1) and, importantly, they were further improved by increasing the number of cRGD to 15. It should be noted that such improvement by conjugating more than 10 cRGDs to one molecule was rarely reported[120] presumably because of difficulty in synthesis or poor hydrophilicity caused by the massive number of cRGD peptides. In this study, I utilized highly hydrophilic PEG-PGlu as a platform; more than 10 cRGD peptides could be conjugated to one construct, revealing that 15 cRGD peptides permit further improvement in cellular uptake and targeting ability (Figure 3.3.1).

3.3.2 Cell viability assay

Successful PDT requires high phototoxicity and minimal dark toxicity. Cytotoxicity of the PSs in U87MG and K562 cells was evaluated by Cell Counting Kit-8 assay (Figure 3.3.2). Free 700DX, 700DX-PEG-cRGD, and 700DX-PEG-PGlu-cRAD exhibited ignorable dark toxicity in U87MG cells while 700DX-PEG-PGlu-cRGD5 showed slight cytotoxicity depending on concentration, and 700DX-PEG-PGlu-cRGD15 moderately reduced the cell viability (Figure 3.3.2a).

Meanwhile, all the PSs did not show dark toxicity in K562 cells (Figure 3.3.2b). The dark toxicity of 700DX-PEG-PGlu-cRGD5 and 700DX-PEG-PGlu-cRGD15 in U87MG cells might be attributed to cell detachment and apoptosis induced by high concentration of cRGD peptides as previously reported[121]. As shown in Figure 3.3.2c, for the U87MG cells, free 700DX and 700DX-PEG-PGlu-cRAD15 did not show phototoxicity, which is in line with the low cellular uptake in Figure 3.3.1 and a previous study reporting negligible PDT effect of 700DX without antibodies[115]. It is noteworthy that 700DX-PEG-cRGD also exhibited little phototoxicity while it demonstrated the considerably enhanced cellular uptake (Figure 3.3.1), suggesting that the cellular uptake offered by monomeric cRGD peptide might be insufficient to induce photochemical damage in this experimental condition. Consistent with these results, 700DX-PEG-PGlu-cRGD5 and 700DX-PEG-PGlu-cRGD15 at low concentration failed to induce PDT effect. However, they drastically exhibited phototoxicity at high concentration, where their cellular uptake was significantly increased. Interestingly, although cellular uptake of 700DX-PEG-PGlu-cRGD5 at 100 nM was similar to that of 700DX-PEG-cRGD at 200 nM, 700DX-PEG-PGlu-cRGD5 obviously excelled at phototoxicity. Considering their similar cellular uptake and subcellular localization, this enhanced phototoxicity might be explained by the combinatorial effect of PDT and the aforementioned cytotoxicity induced by cRGD peptides. Different from these results obtained in U87MG cells, phototoxicity could not be observed in K562 cells even at high PS concentration (Figure 3.3.2d), which is also in good agreement with the cellular uptake as discussed above. These results indicate that multiple cRGD peptides-conjugated 700DX can induce strong toxicity only to the target cells without untoward damage to the non-target cells even under photoirradiation.

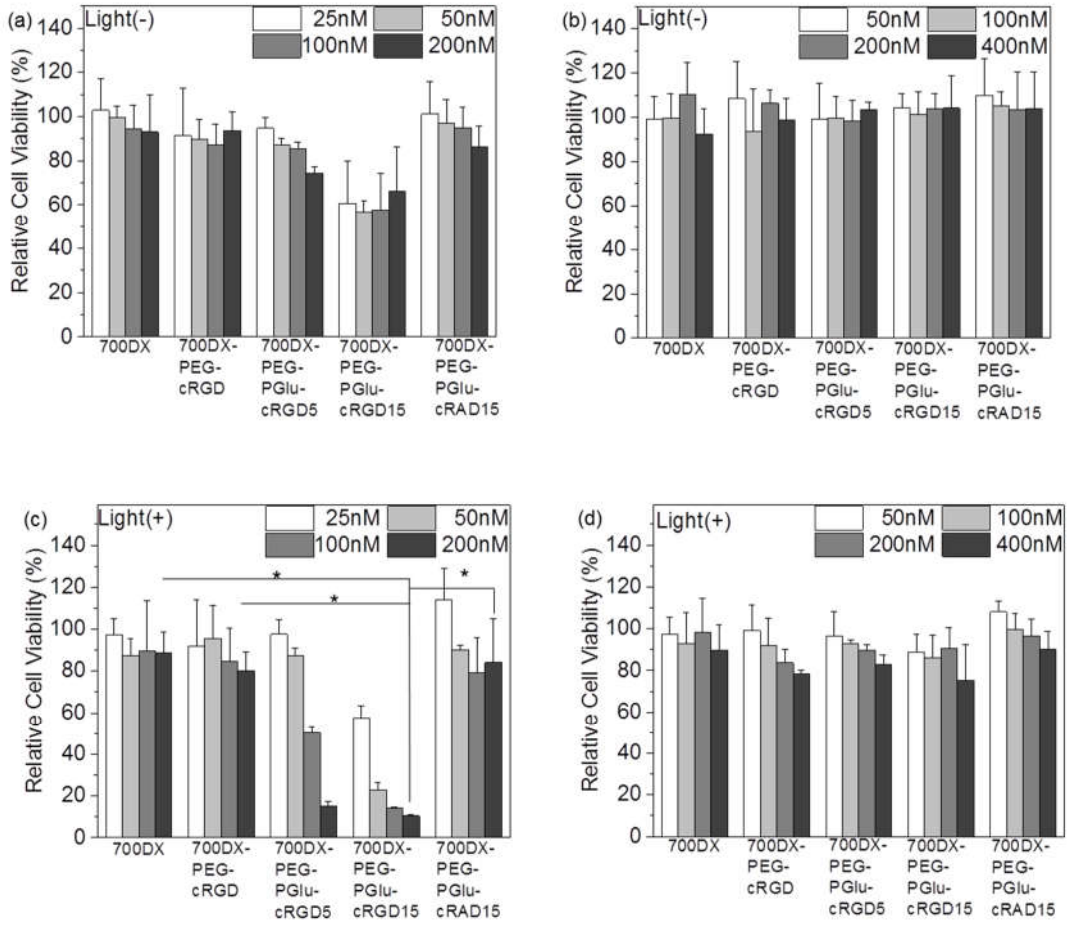

Figure 3.3.2. Dark toxicity and phototoxicity of PSs in (a, c) U87MG and (b, d) K562 cells.

For the application of PS, the systemic phototoxicity was an important limitation. After conjugated with the polymer, the PS has shown high phototoxicity to the targeting tumor cells, and almost no toxicity to non-targeting cells even at higher concentration. The dark toxicity to both cell lines all and phototoxicity to non-targeting cell line suggested PS-polymer conjugates has no material toxicity and systemic phototoxicity. At the same time, targeting ability could increase the PS concentration without increasing the amount of PS, compared to free PS. The decreased amount of necessary PS might further reduce the phototoxicity of the PDT.

3.3.3 Biodistribution

To examine the biodistribution of the PSs, I observed localization of the intravenously injected PSs in mice bearing subcutaneous U87MG tumors using in vivo imaging system (IVIS) (Figure 3.3.3a), and quantified the amount of the PSs in the tumors and normal organs by measuring the fluorescence intensity of PSs in their homogenized solutions (Figure 3.3.3b and Figure 3.3.4). Free 700DX and 700DX-PEG-PGlu-cRAD15 did not show tumor-specific accumulation and quickly disappeared from the body possibly through renal clearance as indicated by the high accumulation to the kidney (Figure 3.3.4b). Although the tumor accumulation of 700DX-PEG-cRGD was slightly higher than free 700DX and 700DX-PEG-PGlu-cRAD15, the accumulation level was comparable to those in normal organs, which may be because of the insufficient affinity of monomeric cRGD peptide and eventual washout from the target site as reported by a previous study[122]. By contrast, 700DX-PEG-PGlu-cRGD5 and 700DX-PEG-PGlu-cRGD15 exhibited significantly enhanced tumor accumulation compared with the other PSs, and their accumulation level in the tumor was higher than those in the normal organs including liver, lung, spleen, muscle, and skin. Moreover, 700DX-PEG-PGlu-cRGD15 revealed high tumor accumulation level even 6 and 24 h after the injection. These results suggest the improved affinity to $\alpha_v\beta_3$ integrin by multivalent effect[123] and its usability to deliver 700DX to the target tumor. It should be noted that conjugation of multiple cRGD peptides to 700DX did not increase the accumulation level in the normal organs except for the kidney that should be the main elimination route through glomerular filtration, and the rapid renal clearance led to the quick disappearance of the PS from the blood (Figure 3.3.4). The rapid clearance from the blood consequently increased tumor/blood accumulation ratio of the PS (Figure 3.3.5), which is beneficial to avoid untoward photochemical damage to normal tissue including photosensitivity.

(a)

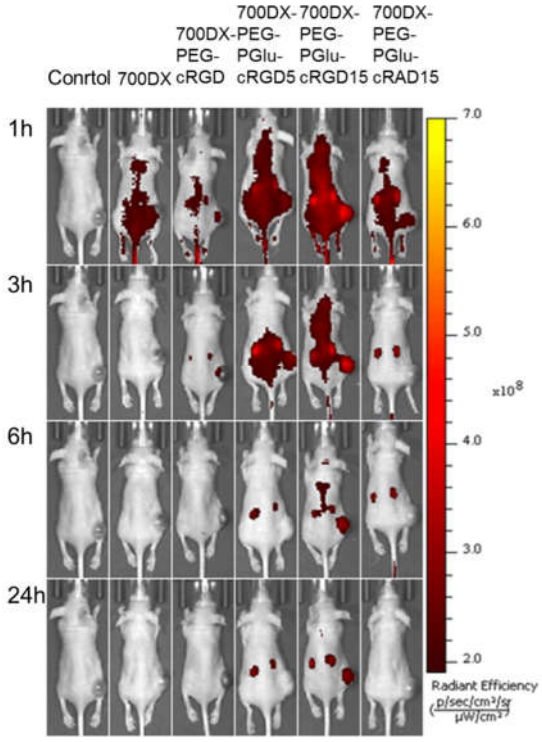

(b)

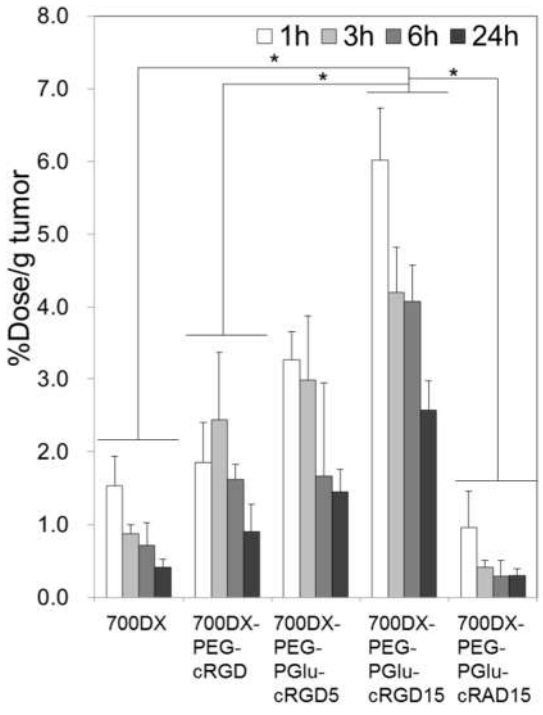

Figure 3.3.3. Biodistribution of PSs. (a) IVIS images obtained at 1, 3, 6 and 24h after injection. (b) Biodistribution of PSs in tumor quantified by fluorescence intensity and expressed as a percentage of the injected dose/g tissue.

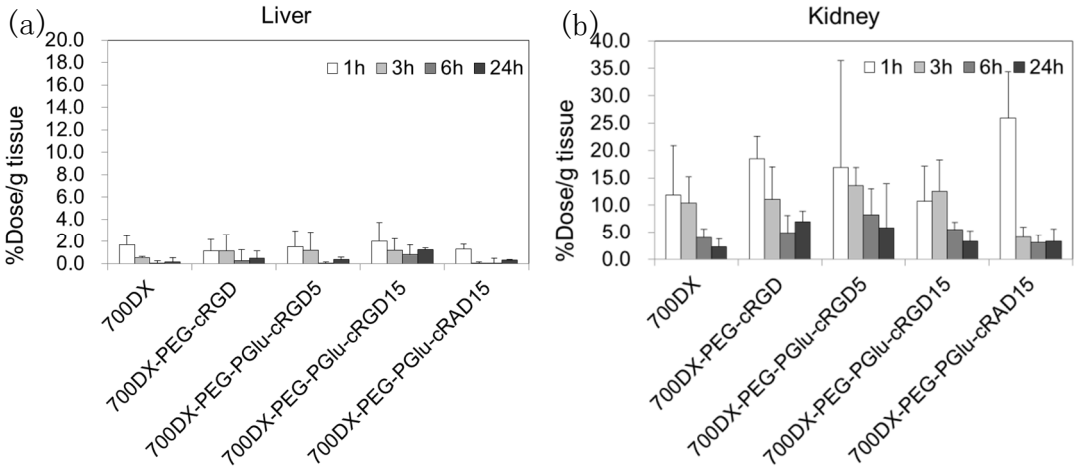

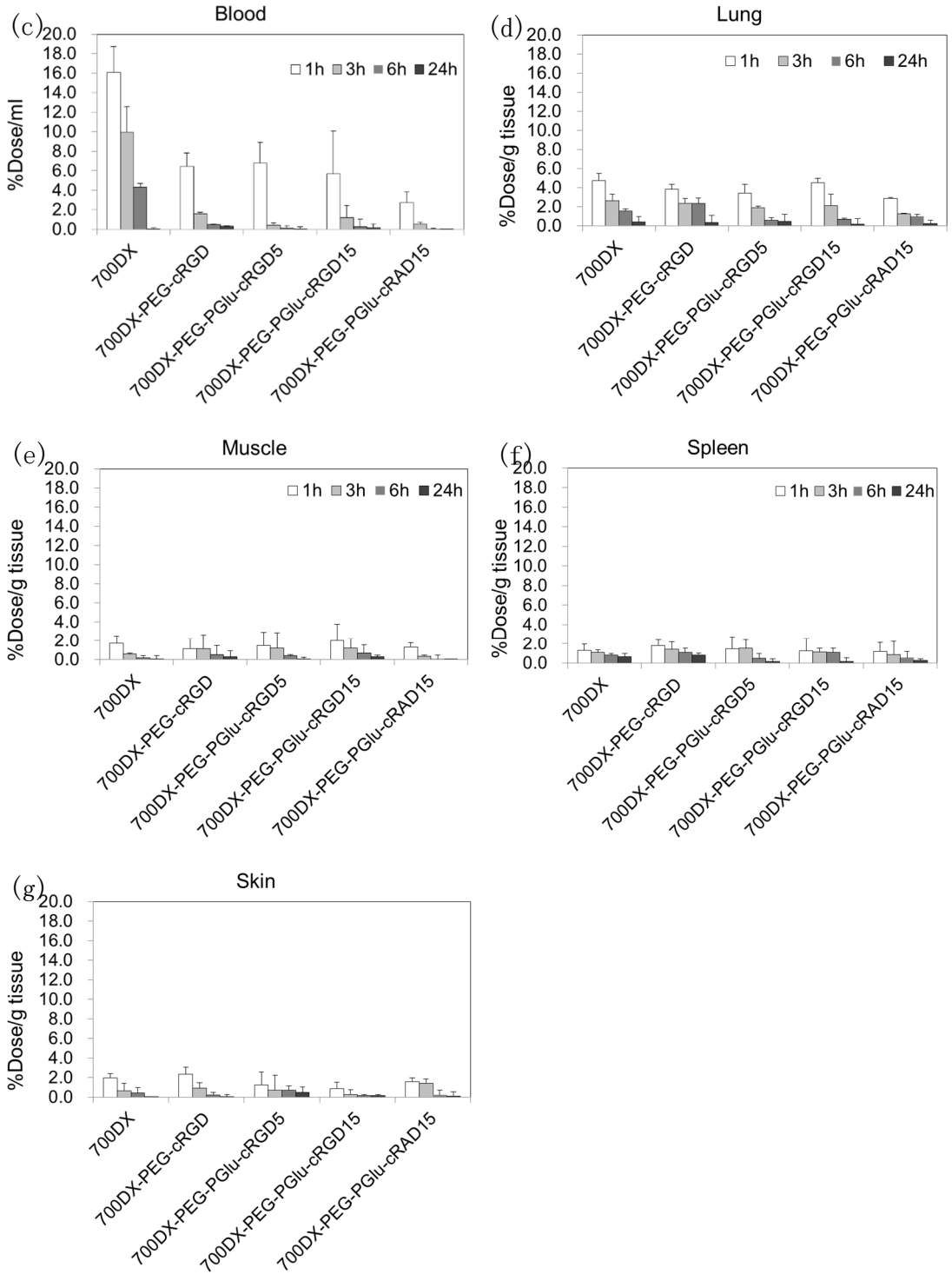

Figure 3.3.4. Biodistribution study. Accumulation of PSs in (a) liver, (b) kidney, (c) blood, (d) lung, (e) muscle, (f) spleen, and (g) skin.

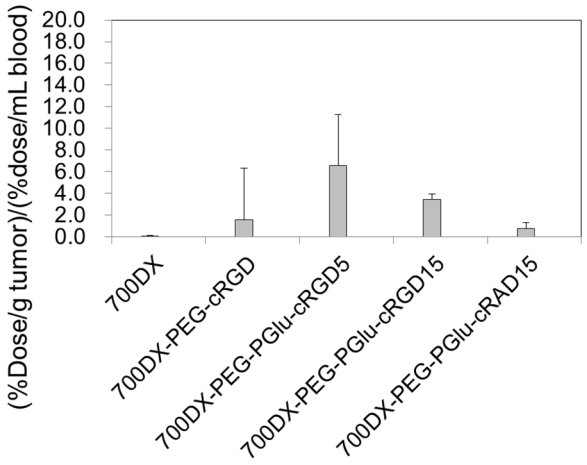

Figure 3.3.5. Tumor/blood accumulation ratio of PSs 3h after injection.

3.3.4 Intratumoral distribution

Intratumoral distribution of the PSs 3 h after injection was investigated by observing tumor tissue by CLSM (Figure 3.3.6). Consistent with tumor accumulation result (Figure 3.3.3), the U87MG tumors treated with 700DX-PEG-PGlu-cRGD5 and 700DX-PEG-PGlu-cRGD15 exhibited appreciably higher fluorescence intensity than those treated with free 700DX and 700DX-PEG-PGlu-cRAD15. Monomeric cRGD also improved the accumulation of 700DX; however, compared with 700DX-PEG-PGlu-cRGD5 and 700DX-PEG-PGlu-cRGD15, its tumor accumulation was limited. These results again illustrate the higher tumor accumulation of the 700DX-PEG-PGlu-cRGD5 and 700DX-PEG-PGlu-cRGD15 via the enhanced avidities to $\alpha_v\beta_3$ integrin. In addition to the enhanced accumulation, these multiple cRGD-conjugated PSs revealed unique intratumoral distribution. Both of the 700DX-PEG-PGlu-cRGD5 and 700DX-PEG-PGlu-cRGD15 accumulated within tumor cells as well as tumor-associated vasculature, and 700DX-PEG-PGlu-cRGD15 was more preferentially localized on the vasculature without compromising penetration to a deep region. These results suggest that intratumoral distribution can be controlled by fine-tuning the number of cRGD peptides.

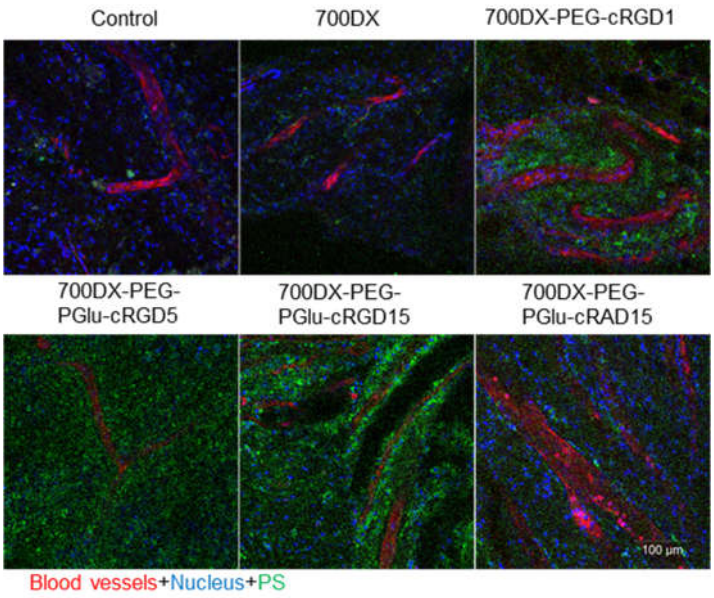

Figure 3.3.6. Representative CLSM images of intratumoral distribution of PSs.

Although the cRGD modified polymer or nanoparticles showed high penetration in the previous studies[124-126], delivery to cells that are distal from functioning blood vessels may be still limited by irregular blood flow, the compression of blood vessels, increased interstitial fluid pressure, heterogeneous $\alpha_v\beta_3$ integrin expression and structure of the extracellular matrix[127]. Thus, elimination of all the tumor cells is sometimes difficult only by directly giving oxidative damage to tumor cells in PDT. In this regard, many studies suggested that the tumor-associated vasculature targeted PDT could enhance the therapeutic efficacy[128]. By shutting down tumor-associated vasculature, cells surviving the direct oxidative damage should be killed by lack of oxygen and nutrition. However, conventional PSs do not have selectivity to the tumor-associated vasculature. To conduct the tumor-associated vasculature targeted PDT, the light should be delivered while blood contains the high concentration of PS, which also damages blood vessels in normal tissues. To selectively damage tumor-associated vasculature, the PS should be delivered to the tumor-associated vasculature and quickly cleared from the blood. In this study, 700DX-PEG-PGlu-cRGD5 and 700DX-PEG-PGlu-cRGD15 could accumulate in the tumor-associated vasculature (Fig. 3.3.3), while the PS in blood was quickly

decreased within 3 h after injection (Figure 3.3.4). Because the molecular weights of 700DX-polymer conjugates were smaller than 40 kDa (threshold of glomerular filtration)[129], the rapid disappearance of 700DX-polymer conjugates in blood should be mediated by renal clearance, as indicated by the high accumulation in the kidney (Figure 3.3.4). Thus, different from the tumor-associated vasculature with high accumulation of the PSs, the normal blood vessels accidentally exposed to photoirradiation are expected to avoid photochemical damage.

3.3.5. In vivo antitumor activity

In vivo antitumor effect of PDT was examined in a subcutaneous U87MG tumor in a mouse (Figure 3.3.7). U87MG tumors were treated with a single dose of photoirradiation [100 mW/cm^2, 1000 sec] 3h after intravenous administration of the PSs. It is evident that all the PSs delayed the tumor growth; however, no statistical significance could be obtained among 700DX, 700DX-PEG-cRGD, and 700DX-PEG-cRAD15. These antitumor effects were consistent with the accumulation result (Figure 3.3.3), suggesting the direct photochemical damage to kill tumor cells was limited by the lower local concentration of PS in the tumor (Figure 3.3.3). Meanwhile, 700DX-PEG-PGlu-cRGD5 and 700DX-PEG-PGlu-cRGD15 significantly inhibited the tumor growth. These high antitumor effects can be partially explained by the high tumor accumulation (Figure 3.3.3). It is noteworthy that 700DX-PEG-PGlu-cRGD15 more remarkably inhibited the growth of tumors than 700DX-PEG-PGlu-cRGD5, although the tumor accumulation of 700DX-PEG-PGlu-cRGD5 and 700DX-PEG-PGlu-cRGD15 was similar 3 h after injection (Figure 3.3.3b). Considering the more preferential accumulation of 700DX-PEG-PGlu-cRGD15 on the tumor-associated vasculature (Figure 3.3.5), the appreciable difference in antitumor effects between 700DX-PEG-PGlu-cRGD5 and 700DX-PEG-PGlu-cRGD15 might be caused by tumor vasculature damage, which may also explain the difference between 700DX-PEG-PGlu-cRGD5 and 700DX-PEG-cRGD. These results suggest that spatial control of 700DX distribution

in the tumor is important to improve PDT effect.

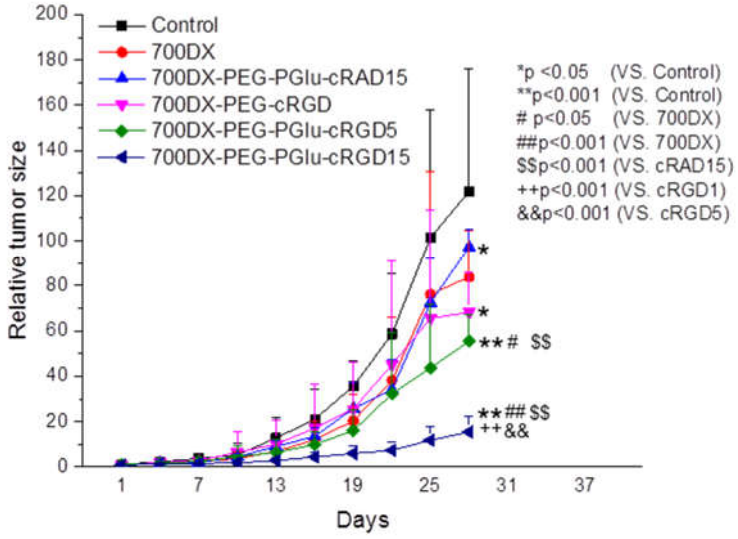

Figure 3.3.7. PDT efficacy of PSs.

The 700DX-PEG-PGlu-cRGD15 demonstrated efficient penetration in the tumor as well as preferential accumulation to the tumor vasculature, thereby accomplishing the efficient antitumor effect. Unlike this study, in some other research about multiple cRGD-conjugated systems[130,131], cRGD conjugated nanoparticles could accumulate only in edge part or near-vessel part of the tumor. The limited penetration of these materials was ascribed to their large size, as reducing the size of cRGD-conjugated nanomaterials could improve the penetration ability[131]. Thus, the small size of the conjugates in the present study might contribute to the high penetration. Another reason for the efficient penetration might be a possible transcytosis pathway through cRGD-integrin mediated active transport. This hypothesis was used to explain high penetration of cRGD-conjugated micelles in 3D U87MG glioma spheroids in a previous research[125]. The micelle covered by cRGDs demonstrated superior efficacy to penetrate into the deeper part of 3D U87MG glioma spheroids compared to similar micelle without cRGD peptide modification. Similar improvement was also observed in other micelle[124] and nanoparticle[126].

To improve the efficacy of PDT, some strategy could be used for references to deepen this research in the future. Some researchers incorporated 700DX into nanocarrier to enhance the selectivity of treatment by promoting tumor targeting with active targeting moieties[132]. Combined therapy with other drug was also an approach to improve the efficacy of PDT[133]. And the PSs could offer a light-enhanced cytosolic release for membrane-impermeable molecular therapeutics in combined therapy, which also is helpful to achieve eradication of tumor.

Conclusion

I developed the 700DX-polymer conjugates containing multiple cRGDs that could show a high affinity to tumor cells overexpressing $\alpha_v\beta_3$ integrin. These conjugates exhibited enhanced cellular uptake in the cultured cells by strong interaction with $\alpha_v\beta_3$ integrin and achieved targeting delivery and prolonged retention at tumor site with controlled intratumoral distribution. Owing to these improvements, the 700DX-polymer conjugates significantly inhibited the growth of tumor. Thus, the multiple cRGD peptides conjugated polymer is a promising structure for PDT of 700DX.

4. Photochemical internalization application for siRNA delivery system

4.1 Introduction

In the previous chapter, I discussed the PS-polymer conjugates could enhance the cellular uptake by promoting the endocytosis. The localization in the endosomes is suitable for photochemical internalization (PCI). As mentioned before, the PCI has been shown to facilitate intracellular delivery of a large variety of macromolecules that do not otherwise readily penetrate the plasma membrane. The PCI technology is based on the same principles as PDT, but different with PDT, the PS should be located in the endocytic vesicles of the targeted cells. After the activation of light, the PS will destroy the membrane of the endosome. Then the macromolecules will later be released before being degraded in lysosomes. This site-specific drug delivery induced by PCI will take place in addition to the well-described cytotoxic, vascular and immunostimulatory effects of PDT.

To test the PCI application potential of the PS-polymer conjugates, small interfering RNA (siRNA) was used as the macromolecules in the study. The siRNA could interfere with the expression of specific genes by degrading mRNA before translation via the RNA interference (RNAi) pathway. Because of the ability to silence any gene of interest, the siRNA was widely applied in the cancer therapy by knocking down cancer-associated mutation gene. Similar to the other antitumor agents, the successful siRNA therapy needs the delivery system. At the same time, intracellular delivery of siRNA also is a great challenge. The mechanism of RNAi pathway decides that the siRNA should be released to cytoplasm from endosome before being destroyed by various enzymes. Delivery system could protect the siRNA by shielding them from enzymes. Enhancing the release by PCI is also a method to protect the siRNA by reducing the time of trapping in the endosome.

In this chapter, confocal laser scanning microscopic observation was also firstly performed to confirm the intercellular location of the PS-polymer. Then, I determined the PCI ability of my PS-polymer conjugates by testing the transfection efficiency of the PS-polymer conjugates/siRNA complex mixture with or without irradiation. These

in vitro results proved the PS-polymer conjugates could be used for PCI.

4.2 Materials and Methods

4.2.1 Materials

All of siRNA, including siGl4-DBCO, Cy5-siRNA-DBCO, and DBCO functioned scramble siRNA (scRNA-DBCO), were purchased from Hokkaido System Science Co., Ltd. (Hokkaido, Japan). Polyethylenimine (linear, average Mn~10,000 Da) was purchased from Tokyo Chemical Industry Co., Ltd. (Tokyo, Japan).

4.2.2 Cell lines

U87MG (human glioblastoma) cell line was purchased from American Type Culture Collection (ATCC) (Manassas, VA). The luciferase-expressing U87MG (U87MG-luc) cell line was obtained from Caliper LifeSciences (Hopkinton, MA). U87MG cells were grown in MEME medium containing 10% FBS and 1% penicillin and streptomycin. Cell lines were incubated at 37℃ in the humidified atmosphere containing 5% CO_2.

4.2.3 Cell viability and Transfection assay

Transfection assays were performed using siGL4 to treat U87MG-luc cell line in the presence of serum. The U87MG-luc cells were seeded in 24-well plates at a density of 10^5 cells in 100 μL of medium/well and incubated for 24 h. The photosensitizes were added into fresh MEME medium, and a series of different concentration solutions were prepared by gradient dilution. The siGL4/PEI complexes at N/P ratio (the ratio of moles of the amine groups of PEI to those of the phosphate ones of siRNA) = 2 were prepared by adding the PEI solution into the siGL4 solution, followed by vortexing and incubation for 30 min at room temperature before using. After 30 mins incubation, the siGL4/PEI complex solution was mixed with MEME medium

containing photosensitizers and the volume of those solutions was adjusted to the same by adding fresh MEME medium. 100 μL medium containing photosensitizers and complex were added to each well to start the 6 h transfection under standard incubator conditions away from light. Then the medium was replaced with 100 μL of the fresh normal medium after washed by PBS once. After 10 mins photoirradiation (0.3 mW/cm_2), the cells were further incubated for an additional 48 h under the same conditions. The other group was treated in the same way but without photoirradiation. Before quantifying the luciferase activity, cell viability was tested by Cell Counting Kit 8 assay. After the cultured cells were washed with PBS 3 times, and lysed in 100 μL of lysis buffer. The lysis buffer was moved to luminescence measurement white plates (Wako Pure Chemical Industries, Ltd. (Osaka, Japan)). Then the luciferase activity was quantified by GLOMAX™ 96 microplate luminometer. The luciferase assay system solution obtained from Promega Corporation (Madison, USA) was automatically mixed with lysis solution by the luminometer.

4.2.4 Fluorescence Microscopy

For photochemical internalization studies, U87MG cells were seeded at a density of 10^5 cells/dish in 35-mm glass-based dishes. After 24 h incubation, cells were incubated in fresh medium containing photosensitizers and cy3-siRNA/PEI complexes for 6 h. Cells were then washed three times by 1 ml of PBS and fixed by PBS containing 4% paraformaldehyde and Hoechst33342 (10 μg/mL). Cells were then observed using a confocal laser scanning microscope (LSM710, Oberkochen, Germany).

Results and Discussion

4.3.1 PCI

Similar to chapter 3.3.1, the subcellular distribution of the PSs was determined by observation of the U87MG cells incubated with the 100 nM PSs (Figure 3.3.1c). Consistent with the cellular uptake shown in Figure 3.3.1c, 700DX-PEG-cRGD5, 700DX-PEG-PGlu-cRGD10, and 700DX-PEG-PGlu-cRGD15 revealed considerably high fluorescence intensity in the cells compared to free 700DX. Importantly, in the cell treated without irradiation, all the PSs were colocalized with Lysotracker Red DND-99. This phenomenon showed the potential of the PS-polymer conjugates used as PCI agents. After exposure to the light, the PS and Lysotracker could not be found in the cell treated with 700DX-PEG-PGlu-cRGD10 and 700DX-PEG-PGlu-cRGD15. On the other hand, the cells incubated with free 700DX and 700DX-PEG-cRGD5 showed no differences after irradiation. These results revealed the disruption of endosomes only happened in the cells treated with 700DX-PEG-PGlu-cRGD10 and 700DX-PEG-PGlu-cRGD15. This phenomenon might be caused by the increased affinity to the integrin. The most important part of PCI is giving the damage to the membrane of endosomes. Since travel distance of ROS created by PS is only several ten nanometers in cells[116], the PS should be localized around the membrane. Some PS could embed in the membrane by their appropriate hydrophobicity. But the PS used in this work is hydrophilic. Hence, the PS was considered to be fixed at the membrane by the cRGD functioned polymer. The multiple cRGD structure could enhance the endocytic process via indenting the cell membrane inward, to increase cellular uptake. After the formation of endosomes, the PS-polymer conjugates with high affinity to the integrin could adhere to the membrane. Only the adhered PS could break the membrane. This hypothesis may explain why free and 700DX-PEG-PGlu-cRGD5 could not achieve the PCI. Increasing the affinity probably could reduce the concentration of PS in the endosomes, which could reduce the damage of ROS to the

therapeutic agents.

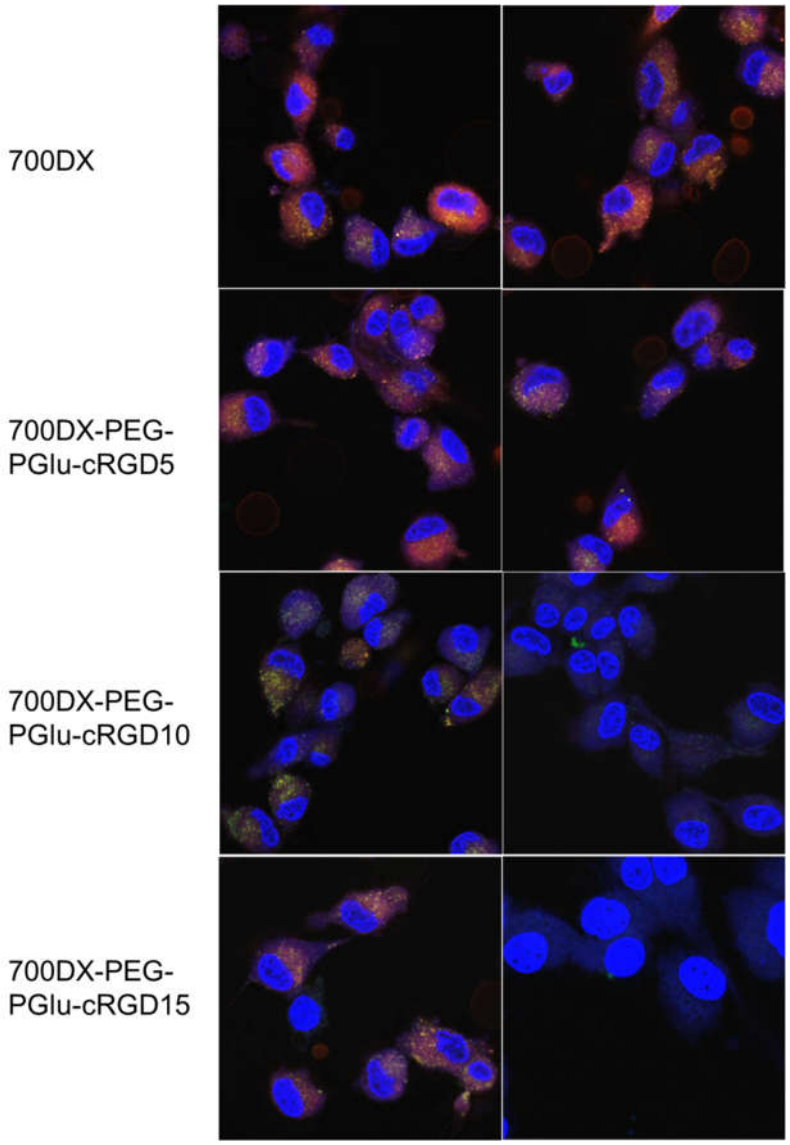

Figure 4.3.1. Confocal microscopy image of U87MG cells treated with PSs. (Green: 700DX; Red: lysotracker; Blue: Hoechst, left: without illumination, right: with 10 mins illumination).

4.3.2 Cell viability and Transfection assay

A successful delivery system should demonstrate high transfection efficiency and compromised toxicity at the same time. Figure 4.3.2a,c shows the in vitro CCK-8 assay results of cytotoxicity of PEI/siRNA complex/PS-polymer conjugates mixture in U87MG-luc cell lines at various PS concentrations without or with irradiation. The dose-dependent cytotoxicity effect was not obvious, suggested PS-polymer has high biocompatibility. For the dark toxicity, only the cells treated with 50nM and 100nM 700DX-PEG-PGlu-cRGD15 shown higher death rate. Compared to the toxicity results in chapter 3, 10 mins irradiation will not lead to cell death. Hence, this PCI method is safe for the siRNA therapy. But for the cancer therapy, additional toxicity from PS is considered beneficial.

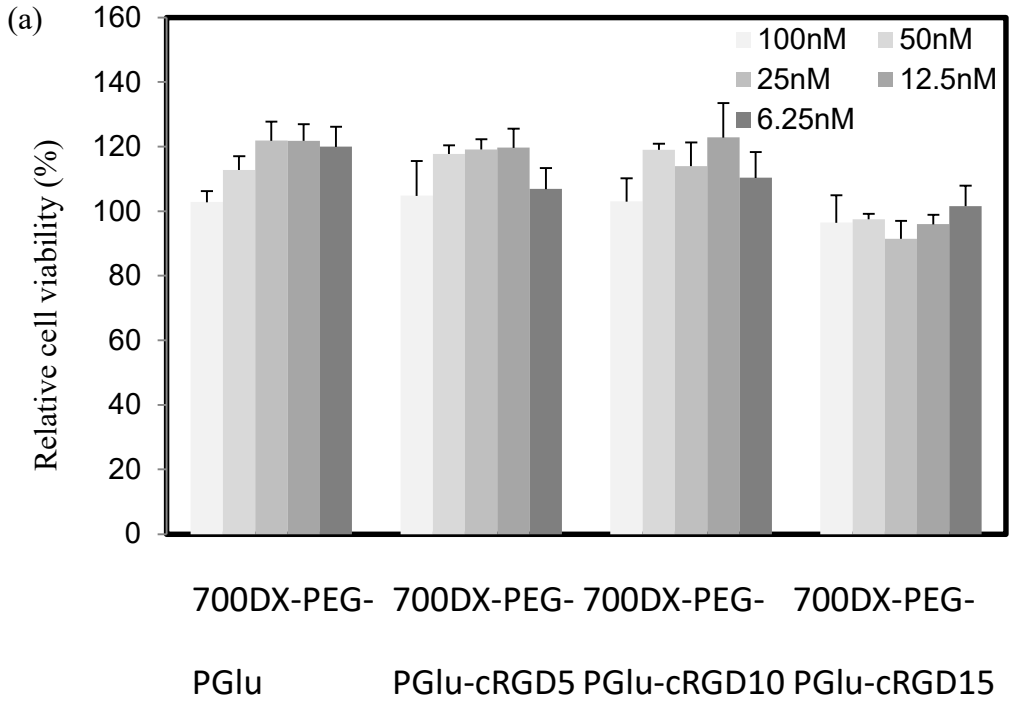

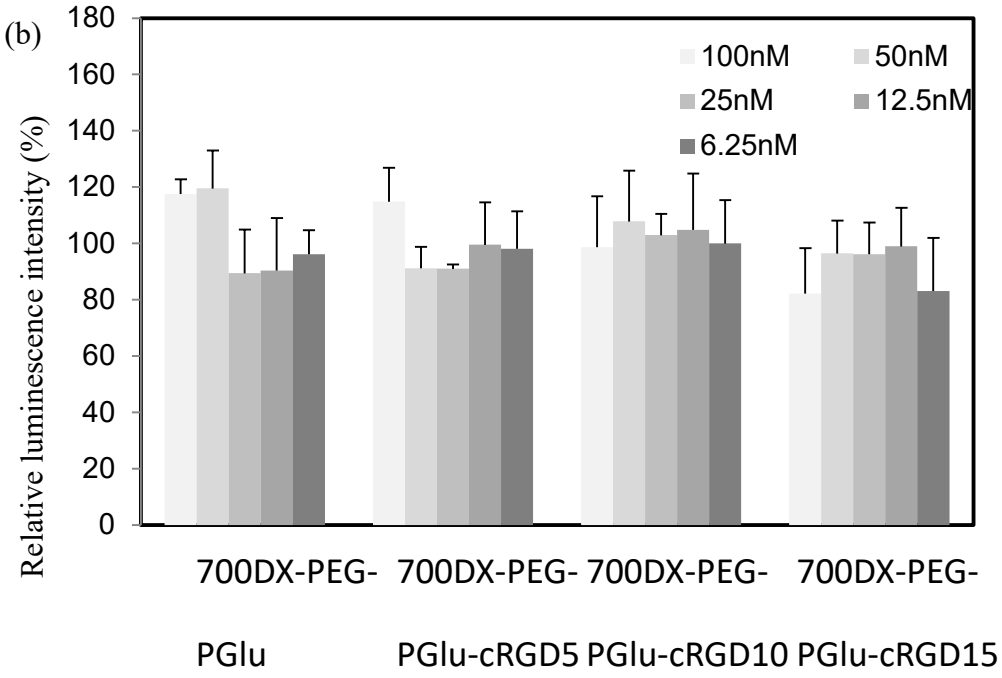
(b)
Relative luminescence intensity (%)
180
160
140
120
100
80
60
40
20
0
100nM
50nM
25nM
12.5nM
6.25nM
700DX-PEG-PGlu
700DX-PEG-PGlu-cRGD5
700DX-PEG-PGlu-cRGD10
700DX-PEG-PGlu-cRGD15

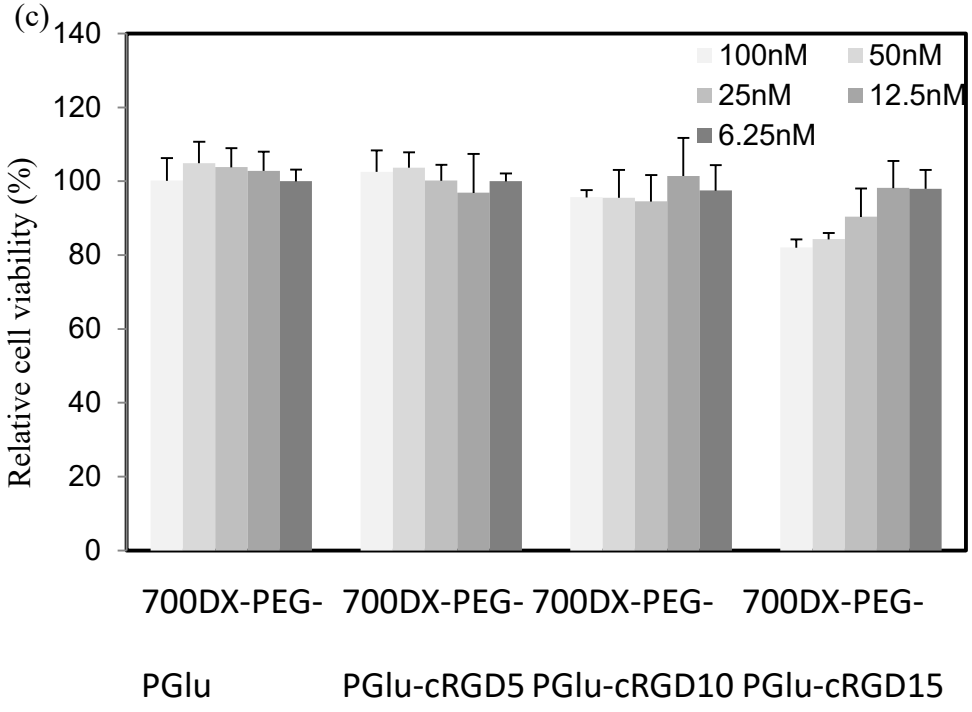
(c)
Relative cell viability (%)
140
120
100
80
60
40
20
0
100nM
50nM
25nM
12.5nM
6.25nM
700DX-PEG-PGlu
700DX-PEG-PGlu-cRGD5
700DX-PEG-PGlu-cRGD10
700DX-PEG-PGlu-cRGD15

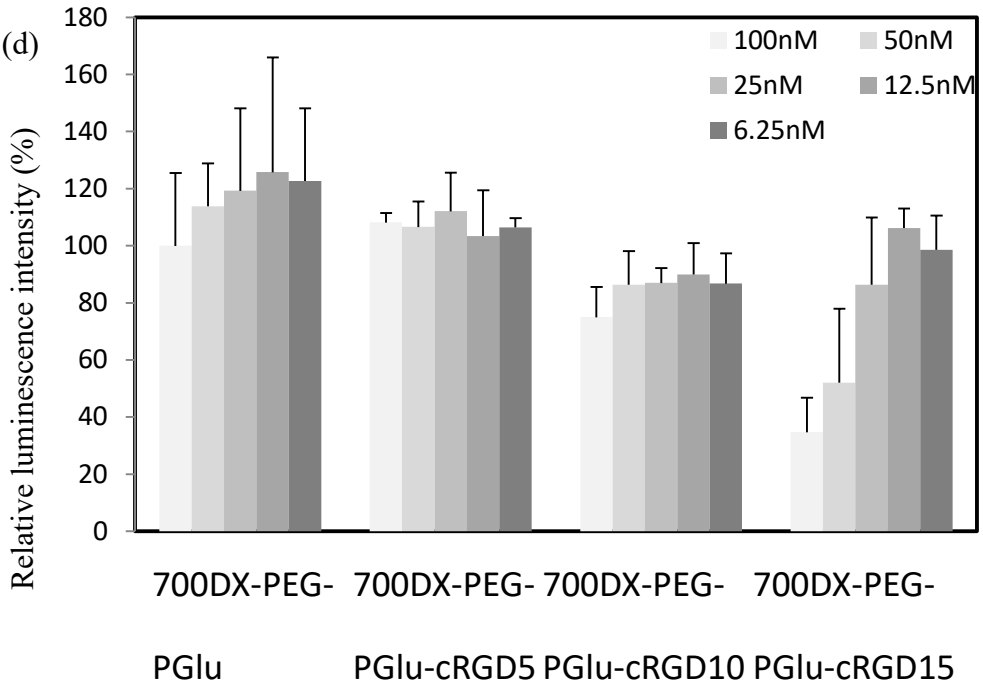

Figure 4.3.2. Cell viability of U87MG-luc cells treated with siRNA/PEI (N/P=2, 2.5nM) and different concentrations of 700DX-cRGDs without illumination (a) and with illumination (c). Relative luminescence intensity without illumination (b) and with illumination (d).

A high concentration of amino groups is always considered an important factor leading to high cytotoxicity. A famous example is the PEI, used as cationic polymers in this work. Normal method to reduce the cytotoxicity of PEI is modifying it by biocompatible materials. The PS-polymer conjugates could also reduce the toxicity of PEI/siRNA complex by decreasing the necessary amount. Compared with the Figure 4.3.2b and 4.3.2d, the irradiation enhanced the transfection efficacy in the cell treated with 700DX-PEG-PGlu-cRGD10 and 700DX-PEG-PGlu-cRGD15. The low concentration of PEI/siRNA complex shown no transfection efficacy, but PCI could enhance the transfection efficacy heavily.

Similar to PDT, PSs used in PCI should preferentially accumulate in the tumor and only induce the cytotoxic reaction in it. However, the free PSs could not meet the

targeting delivery demand. Hence, antibodies, receptor ligands, and peptides were used to improve the specificity of PCI treatment. In this study, the structure containing the increased number of cRGD peptides could augment cellular uptake, tumor specificity, and tumor retention of PSs. This structure also brings another benefit that hydrophilic PSs could also be used in PCI. It is generally recognized that PSs having an amphiphilic structure with a hydrophilic part show the most efficacy in PCI. The hydrophilic part could fix the PSs in the hydrophobic tail layer by inhibiting penetration through cellular membranes. The ROS generated by the fixed PSs could directly break the membrane. The hydrophilic PSs distributing in the endocytic vesicles scarcely gave the damage to the membrane, because of the short action range of ROS. In my study, the hydrophilic PS 700DX fixed on the membrane by the integrin-peptide interaction. After the conjugation to the polymer, 700DX had the ability to induce the PCI. Therefore, the structure could increase the candidates of PCI by offer the affinity to integrin on the membrane to hydrophilic PSs.

Conclusion

I developed the 700DX-polymer conjugates containing multiple cRGDs by the method mentioned in chapter 2. After exposure to the light, the endosome in the cells treated with 700DX-PEG-PGlu-cRGD10, and 700DX-PEG-PGlu-cRGD15 were broken. The endosome in the cells treated with 700DX and 700DX-PEG-PGlu-cRGD5 have existed. These result proved that after conjugated with the structure containing multiple cRGD peptides, the 700DX has the ability to induce the PCI. Owing to the ability, the 700DX-polymer conjugates could increase the transfection efficiency of PEI/siRNA.

Chapter 5. Summary of the Dissertation

5.1 Summary of the Dissertation

PDT has attracted a lot of interest as a potential cancer therapy. But the successful PDT application is still limited by several problems. To overcome the main one of these problems, non-cancer cell targeting, biomolecules were involved in the PS delivery system. This study focused on the development of the PS-polymer conjugates containing multiple cRGD peptides, characterization of polymer structure and affinity to tumor cells through multivalent effect, and their biological performance *in vitro* and *in vivo*.

Synthesis and characterization of PS-polymers conjugates were discussed in chapter 2. After ring-opening polymerization of N-carboxy anhydride (NCA), deprotection reaction, side chain conjugation reaction between carboxyl groups of PGlu and amine groups of cRGD, and introduction of PS to the polymer terminus, the PS-polymer conjugates were synthesized. Through the side chain conjugation reaction, the target number of cRGD peptides was conjugated to the azide-PEG-PGlu with narrow molecular weight distribution. The same method was used to synthesize the control material. PS was conjugated to the polymer terminus and purified by HPLC. After these steps, PS-polymer conjugates showed monodisperse molecular weight distribution, proving the stability of the conjugates.

Biological performances of the PS-polymer conjugates in *in vitro* and *in vivo* were assessed in chapter 3. Cellular uptake of the PS-polymer conjugates was analyzed by IVIS and confocal microscope to investigate the interaction between multiple cRGD and integrin. The 700DX-PEG-cRGD, 700DX-PEG-PGlu-cRGD5, and 700DX-PEG-PGlu-cRGD15 revealed significantly high cellular uptake depending on the number of cRGD peptides, while no significant difference could be obtained between free 700DX and 700DX-PEG-PGlu-cRAD15. In addition, PSs were internalized into the cells via an endocytic process. The high cellular uptake efficiency of 700DX-PEG-PGlu-cRGD15 compared 700DX-PEG-cRGD, free 700DX, and 700DX-PEG-PGlu-cRAD15 might be attributed to the high affinity to integrin. The

high affinity also enhanced the tumor targeting ability, tumor retention time and antitumor effect.

In chapter 3, I found the PS-polymer conjugates localized in the endosomes, suggesting it had the potential to be used as the agent for PCI. To confirm this hypothesis, cells treated with PS-polymer conjugates were exposed to light in chapter 4. In the cell treated without irradiation, all the PSs were localized in endosomes. After exposure to the light, the PS and lysotracker could not be found in the cell treated with 700DX-PEG-PGlu-cRGD10 and 700DX-PEG-PGlu-cRGD15, suggesting broken of endosomes happened in the cells treated with them. The cells incubated with free 700DX and 700DX-PEG-cRGD5 showed no differences before and after irradiation. By this ability, PS-polymer conjugates could enhance the transfection efficacy heavily, or reduce the toxicity of PEI/siRNA complex by decreasing the necessary amount.

Overall, I developed the multiple cRGD-functionalized polymers with a high affinity to tumor cells overexpressing avb3 integrin. After conjugated them with PS, I found PS-polymer conjugates exhibited enhanced cellular uptake, tumor target ability and prolonged tumor retention. Beside the PDT application, the PS-polymer conjugates also had potential in PCI application.

5.2 Future perspectives

In this work, I synthesized a 700DX-polymer conjugate having multimeric cRGD peptides. The establishment of multimeric cRGD peptides structure is one way to overcome the disadvantages of monomeric cRGD. However common dendrimer structure could form diploid, tetraploid, and triploid. There is only one reference mentioned dendrimer structure containing 16 cRGD without cell experiments and animal experiments. The problems caused by the hydrophobicity of the dendrimer multiple cRGD peptides structure doesn’t limit the application of the linear structure. These conjugates exhibited enhanced cellular uptake in the cultured cells by strong

interaction with $\alpha_v\beta_3$ integrin and achieved targeting delivery and prolonged retention and heavy inhibition of the growth of the tumor. In addition, intratumoral distribution results suggest that intratumoral distribution can be controlled by fine-tuning the number of cRGD peptides. Considering this intratumoral distribution of PSs, inhibition of tumor growth may be caused by direct tumor cell damage and tumor vasculature damage. These results suggest that spatial control of 700DX distribution in the tumor is important to improve PDT effect. Therefore, the development of PS delivery system should not only focus on one mechanism of tumor destruction. This study suggested that improving the mechanisms at the same time should be a method to develop potential PDT. Thus, the multiple cRGD peptides conjugated polymer is a promising structure for PDT. In this work, the PS is hydrophilic. And I speculate this polymer could better the application of some hydrophobic PSs by offering the hydrophilicity to them. At the same time, changing the cRGD peptide to other kind peptides or biomolecules could also expand the application of this polymer.

Photochemical internalization application is another application of the PS-polymer conjugates. In most gene therapy, the therapeutic gene is taken into the cell by endocytosis, and the lack of efficient mechanisms for enhancing endosomal escape limited the realization of the therapeutic potential of the gene. PCI is a novel technology to improve the therapeutic effect of gene therapy by enhancing the release of DNA or siRNA accumulated in endocytic vesicles. The in vitro experiment confirmed the ability of the conjugates to break the membrane of endosome to release the siRNA/PEI complex. The novel PS-polymer conjugates is a success active-targeting PCI agent and might have the potential to achieve the PIC in in vivo.

References

1 Yavari, N., Andersson-Engels, S., Segersten, U. & Malmstrom, P.-U. An overview on preclinical and clinical experiences with photodynamic therapy for bladder cancer. *Canadian Journal of Urology* **18**, 5778 (2011).

2 Allison, R., Moghissi, K., Downie, G. & Dixon, K. Photodynamic therapy (PDT) for lung cancer. *Photodiagnosis and photodynamic therapy* **8**, 231-239 (2011).

3 Green, B., Cobb, A. R. & Hopper, C. Photodynamic therapy in the management of lesions of the head and neck. *British Journal of Oral and Maxillofacial Surgery* **51**, 283-287 (2013).

4 Schweitzer, V. G. Photodynamic therapy for treatment of head and neck cancer. *Otolaryngology—Head and Neck Surgery* **102**, 225-232 (1990).

5 Biel, M. A. Photodynamic therapy and the treatment of head and neck neoplasia. *The Laryngoscope* **108**, 1259-1268 (1998).

6 Dougherty, T. J. *et al.* Photoradiation in the Treatment of Recurrent Breast Carcinoma 2. *Journal of the National Cancer Institute* **62**, 231-237 (1979).

7 Mang, T. S., Allison, R., Hewson, G., Snider, W. & Moskowitz,

R. A phase II/III clinical study of tin ethyl etiopurpurin (Purlytin)-induced photodynamic therapy for the treatment of recurrent cutaneous metastatic breast cancer. *The cancer journal from Scientific American* **4**, 378-384 (1998).

8 Dimofte, A., Zhu, T. C., Hahn, S. M. & Lustig, R. A. In vivo light dosimetry for motexafin lutetium‐mediated PDT of recurrent breast cancer. *Lasers in surgery and medicine* **31**, 305-312 (2002).

9 Ward, B. G., Forbes, I. J., Cowled, P. A., McEvoy, M. M. & Cox, L. W. The treatment of vaginal recurrences of gynecologic malignancy with phototherapy following hematoporphyrin derivative pretreatment. *American journal of obstetrics and gynecology* **142**, 356-357 (1982).

10 Hornung, R. Photomedical approaches for the diagnosis and treatment of gynecologic cancers. *Current Drug Targets-Immune, Endocrine & Metabolic Disorders* **1**, 165-177 (2001).

11 Fehr, M. K. *et al.* Photodynamic therapy of vulvar intraepithelial neoplasia III using topically applied 5-aminolevulinic acid. *Gynecologic oncology* **80**, 62-66 (2001).

12 Gomer, C. J., Doiron, D. R., Jester, J. V., Szirth, B. C. &

Murphree, A. L. Hematoporphyrin derivative photoradiation therapy for the treatment of intraocular tumors: examination of acute normal ocular tissue toxicity. *Cancer research* **43**, 721-727 (1983).

13 Favilla, I. *et al.* Photodynamic therapy: a 5-year study of its effectiveness in the treatment of posterior uveal melanoma, and evaluation of haematoporphyrin uptake and photocytotoxicity of melanoma cells in tissue culture. *Melanoma research* **5**, 355-364 (1995).

14 Landau, I. M., Steen, B. & Seregard, S. Photodynamic therapy for circumscribed choroidal haemangioma. *Acta Ophthalmologica* **80**, 531-536 (2002).

15 Sandeman, D. Photodynamic therapy in the management of malignant gliomas: a review. *Lasers in Medical Science* **1**, 163-174 (1986).

16 Hill, J. S. *et al.* Selective uptake of hematoporphyrin derivative into human cerebral glioma. *Neurosurgery* **26**, 248-254 (1990).

17 Popovic, E. A., Kaye, A. H. & Hill, J. S. Photodynamic therapy of brain tumors. *Journal of clinical laser medicine & surgery* **14**, 251-261 (1996).

18 Rosenthal, M. A. *et al.* Phase I and pharmacokinetic study of

photodynamic therapy for high-grade gliomas using a novel boronated porphyrin. *Journal of clinical oncology* **19**, 519-524 (2001).

19 Barr, H., Krasner, N., Boulos, P., Chatlani, P. & Bown, S. Photodynamic therapy for colorectal cancer: a quantitative pilot study. *British Journal of Surgery* **77**, 93-96 (1990).

20 MÍkvy, P. *et al.* Photodynamic therapy for gastrointestinal tumors using three photosensitizers--ALA induced PPIX, Photofrin and MTHPC. A pilot study. *Neoplasma* **45**, 157-161 (1998).

21 Kostovic, K. *et al.* Photodynamic therapy in dermatology: current treatments and implications. *Collegium antropologicum* **36**, 1477-1481 (2012).

22 Allison, R. R., Mang, T. S. & Wilson, B. D. in *Seminars in cutaneous medicine and surgery.* 153-163 (WB Saunders).

23 Taber, S. W., Fingar, V. H., Coots, C. T. & Wieman, T. J. Photodynamic therapy using mono-L-aspartyl chlorin e6 (Npe6) for the treatment of cutaneous disease: a Phase I clinical study. *Clinical cancer research* **4**, 2741-2746 (1998).

24 Delaney, T. F. *et al.* Phase I study of debulking surgery and photodynamic therapy for disseminated intraperitoneal tumors. *International Journal of Radiation Oncology* Biology**

Physics **25**, 445-457 (1993).

25 Pass, H. I. *et al.* Intrapleural photodynamic therapy: results of a phase I trial. *Annals of surgical oncology* **1**, 28-37 (1994).

26 Ortner, M. A. E. *et al.* Photodynamic therapy of nonresectable cholangiocarcinoma. *Gastroenterology* **114**, 536-542 (1998).

27 Bown, S. *et al.* Photodynamic therapy for cancer of the pancreas. *Gut* **50**, 549-557 (2002).

28 Muragaki, Y. *et al.* Phase II clinical study on intraoperative photodynamic therapy with talaporfin sodium and semiconductor laser in patients with malignant brain tumors. *Journal of neurosurgery* **119**, 845-852 (2013).

29 Rigual, N. R. *et al.* Adjuvant intraoperative photodynamic therapy in head and neck cancer. *JAMA Otolaryngology–Head & Neck Surgery* **139**, 706-711 (2013).

30 Friedberg, J. S. *et al.* Phase II Trial of Pleural Photodynamic Therapy and Surgery for Patients With Non–Small-Cell Lung Cancer With Pleural Spread. *Journal of clinical oncology* **22**, 2192-2201 (2004).

31 Akimoto, J., Haraoka, J. & Aizawa, K. Preliminary clinical report on safety and efficacy of photodynamic therapy using talaporfin sodium for malignant gliomas. *Photodiagnosis and photodynamic therapy* **9**, 91-99 (2012).

32 Castano, A. P., Demidova, T. N. & Hamblin, M. R. Mechanisms in photodynamic therapy: part one-photosensitizers, photochemistry and cellular localization. *Photodiagnosis & Photodynamic Therapy* **1**, 279-293 (2004).

33 Josefsen, L. B. & Boyle, R. W. Photodynamic therapy and the development of metal-based photosensitisers. *Metal-Based Drugs* **2008**, 276109 (2008).

34 Dougherty, T. J. *et al.* Photodynamic therapy. *Journal of the National Cancer Institute* **90**, 889-905 (1998).

35 Mroz, P., Yaroslavsky, A., Kharkwal, G. B. & Hamblin, M. R. Cell death pathways in photodynamic therapy of cancer. *Cancers* **3**, 2516-2539 (2011).

36 Dolmans, D. E. *et al.* Vascular accumulation of a novel photosensitizer, MV6401, causes selective thrombosis in tumor vessels after photodynamic therapy. *Cancer research* **62**, 2151-2156 (2002).

37 Abels, C. Targeting of the vascular system of solid tumours by photodynamic therapy (PDT). *Photochemical & photobiological sciences* **3**, 765-771 (2004).

38 Nowis, D. *et al.* The influence of photodynamic therapy on the immune response. *Photodiagnosis and Photodynamic Therapy* **2**, 283-298 (2005).

39 Allison, R. R. & Sibata, C. H. Oncologic photodynamic therapy photosensitizers: a clinical review. *Photodiagnosis & Photodynamic Therapy* **7**, 61 (2010).

40 LIPSON, R. L. & BALDES, E. J. The photodynamic properties of a particular hematoporphyrin derivative. *Archives of dermatology* **82**, 508-516 (1960).

41 Dougherty, T. J. Activated dyes as antitumor agents. *Journal of the National Cancer Institute* **52**, 1333-1336 (1974).

42 Kinsella, T. J., Colussi, V. C., Oleinick, N. L. & Sibata, C. H. Photodynamic therapy in oncology. *Expert opinion on pharmacotherapy* **2**, 917-927 (2001).

43 Lim, C.-K. *et al.* Nanophotosensitizers toward advanced photodynamic therapy of cancer. *Cancer letters* **334**, 176-187 (2013).

44 Boyle, R. W. & Dolphin, D. Structure and biodistribution relationships of photodynamic sensitizers. *Photochemistry and photobiology* **64**, 469-485 (1996).

45 Kato, H. *et al.* Phase II clinical study of photodynamic therapy using mono-L-aspartyl chlorin e6 and diode laser for early superficial squamous cell carcinoma of the lung. *Lung cancer* **42**, 103-111 (2003).

46 Allison, R. R. Photodynamic therapy: oncologic horizons.

Future Oncology **10**, 123-124 (2014).

47 Zhu, T. C. & Finlay, J. C. The role of photodynamic therapy (PDT) physics. *Medical physics* **35**, 3127-3136 (2008).

48 Huang, Z. *et al.* Photodynamic therapy for treatment of solid tumors—potential and technical challenges. *Technology in cancer research & treatment* **7**, 309-320 (2008).

49 Chen, Q. *et al.* Improvement of tumor response by manipulation of tumor oxygenation during photodynamic therapy. *Photochemistry and photobiology* **76**, 197-203 (2002).

50 Huang, Z. *et al.* Hyperoxygenation Enhances the Tumor Cell Killing of Photofrin-mediated Photodynamic Therapy¶. *Photochemistry and photobiology* **78**, 496-502 (2003).

51 Dougherty, T. J. *et al.* Photodynamic therapy. *JNCI: Journal of the National Cancer Institute* **90**, 889-905 (1998).

52 Huang, Y.-Y. *et al.* Can nanotechnology potentiate photodynamic therapy? *Nanotechnology reviews* **1**, 111-146 (2012).

53 Deda, D. K. & Araki, K. Nanotechnology, light and chemical action: an effective combination to kill cancer cells. *Journal of the Brazilian Chemical Society* **26**, 2448-2470 (2015).

54 Mroz, P. *et al.* Photodynamic therapy with fullerenes.

Photochemical & Photobiological Sciences **6**, 1139-1149 (2007).

55 Brown, E. M. B. *et al.* Advancements in using TiO2 bionanoconjugates for precision degradation of intracellular biological structures. *Journal of biomedical nanotechnology* **9**, 539-550 (2013).

56 Ge, J. *et al.* A graphene quantum dot photodynamic therapy agent with high singlet oxygen generation. *Nature communications* **5** (2014).

57 Yamakoshi, Y. *et al.* Active oxygen species generated from photoexcited fullerene (C60) as potential medicines: O2-• versus 1O2. *Journal of the American Chemical Society* **125**, 12803-12809 (2003).

58 Mroz, P. *et al.* Intraperitoneal photodynamic therapy mediated by a fullerene in a mouse model of abdominal dissemination of colon adenocarcinoma. *Nanomedicine: Nanotechnology, Biology and Medicine* **7**, 965-974 (2011).

59 Maksimov, E., Gvozdev, D., Strakhovskaya, M. & Paschenko, V. Hybrid structures of polycationic aluminum phthalocyanines and quantum dots. *Biochemistry* **80**, 323 (2015).

60 Shao, L., Gao, Y. & Yan, F. Semiconductor quantum dots for

biomedicial applications. *Sensors* **11**, 11736-11751 (2011).

61 Zhou, L., Ge, X., Zhou, J., Wei, S. & Shen, J. Multicolor imaging and the anticancer effect of a bifunctional silica nanosystem based on the complex of graphene quantum dots and hypocrellin A. *Chemical Communications* **51**, 421-424 (2015).

62 Bangham, A. Liposomes: the Babraham connection. *Chemistry and physics of lipids* **64**, 275-285 (1993).

63 Vemuri, S. & Rhodes, C. Preparation and characterization of liposomes as therapeutic delivery systems: a review. *Pharmaceutica Acta Helvetiae* **70**, 95-111 (1995).

64 Derycke, A. S. & de Witte, P. A. Liposomes for photodynamic therapy. *Advanced drug delivery reviews* **56**, 17-30 (2004).

65 Lasic, D., Martin, F., Gabizon, A., Huang, S. & Papahadjopoulos, D. Sterically stabilized liposomes: a hypothesis on the molecular origin of the extended circulation times. *Biochimica et Biophysica Acta (BBA)-Biomembranes* **1070**, 187-192 (1991).

66 Ichikawa, K. *et al.* PEGylation of liposome decreases the susceptibility of liposomal drug in cancer photodynamic therapy. *Biological and Pharmaceutical Bulletin* **27**, 443-444 (2004).

67 Rahmanzadeh, R. *et al.* Ki-67 as a molecular target for therapy in an in vitro three-dimensional model for ovarian cancer. *Cancer research* **70**, 9234-9242 (2010).

68 Oku, N. & Ishii, T. Antiangiogenic photodynamic therapy with targeted liposomes. *Methods in enzymology* **465**, 313-330 (2009).

69 Paszko, E., Vaz, G. M., Ehrhardt, C. & Senge, M. O. Transferrin conjugation does not increase the efficiency of liposomal Foscan during in vitro photodynamic therapy of oesophageal cancer. *European Journal of Pharmaceutical Sciences* **48**, 202-210 (2013).

70 Venugopalan, P. *et al.* pH-sensitive liposomes: mechanism of triggered release to drug and gene delivery prospects. *Die Pharmazie* **57**, 659-671 (2002).

71 Dicheva, B. M. & Koning, G. A. Targeted thermosensitive liposomes: an attractive novel approach for increased drug delivery to solid tumors. *Expert opinion on drug delivery* **11**, 83-100 (2014).

72 Yavlovich, A., Smith, B., Gupta, K., Blumenthal, R. & Puri, A. Light-sensitive lipid-based nanoparticles for drug delivery: design principles and future considerations for biological applications. *Molecular membrane biology* **27**, 364-381

(2010).

73 Meers, P. Enzyme-activated targeting of liposomes. *Advanced drug delivery reviews* **53**, 265-272 (2001).

74 Konan, Y. N., Gurny, R. & Allémann, E. State of the art in the delivery of photosensitizers for photodynamic therapy. *Journal of Photochemistry and Photobiology B: Biology* **66**, 89-106 (2002).

75 Avgoustakis, K. *et al.* Effect of copolymer composition on the physicochemical characteristics, in vitro stability, and biodistribution of PLGA–mPEG nanoparticles. *International journal of pharmaceutics* **259**, 115-127 (2003).

76 Beletsi, A., Panagi, Z. & Avgoustakis, K. Biodistribution properties of nanoparticles based on mixtures of PLGA with PLGA–PEG diblock copolymers. *International journal of pharmaceutics* **298**, 233-241 (2005).

77 Panagi, Z. *et al.* Effect of dose on the biodistribution and pharmacokinetics of PLGA and PLGA–mPEG nanoparticles. *International journal of pharmaceutics* **221**, 143-152 (2001).

78 Anderson, J. M. & Shive, M. S. Biodegradation and biocompatibility of PLA and PLGA microspheres. *Advanced drug delivery reviews* **64**, 72-82 (2012).

79 Peng, C.-L. *et al.* Development of pH sensitive

2-(diisopropylamino) ethyl methacrylate based nanoparticles for photodynamic therapy. *Nanotechnology* **21**, 155103 (2010).

80 Wolinsky, J. B. & Grinstaff, M. W. Therapeutic and diagnostic applications of dendrimers for cancer treatment. *Advanced drug delivery reviews* **60**, 1037-1055 (2008).

81 Zhang, G.-D. *et al.* Polyion complex micelles entrapping cationic dendrimer porphyrin: effective photosensitizer for photodynamic therapy of cancer. *Journal of controlled release* **93**, 141-150 (2003).

82 Couleaud, P. *et al.* Silica-based nanoparticles for photodynamic therapy applications. *Nanoscale* **2**, 1083-1095 (2010).

83 Roy, I. *et al.* Ceramic-based nanoparticles entrapping water-insoluble photosensitizing anticancer drugs: A novel drug− carrier system for photodynamic therapy. *Journal of the American Chemical Society* **125**, 7860-7865 (2003).

84 Zhang, R., Wu, C., Tong, L., Tang, B. & Xu, Q.-H. Multifunctional core− shell nanoparticles as highly efficient imaging and photosensitizing agents. *Langmuir* **25**, 10153-10158 (2009).

85 Teng, I.-T. *et al.* Phospholipid-functionalized mesoporous

silica nanocarriers for selective photodynamic therapy of cancer. *Biomaterials* **34**, 7462-7470 (2013).

86 Wieder, M. E. *et al.* Intracellular photodynamic therapy with photosensitizer-nanoparticle conjugates: cancer therapy using a ‘Trojan horse’. *Photochemical & Photobiological Sciences* **5**, 727-734 (2006).

87 Camerin, M. *et al.* The in vivo efficacy of phthalocyanine–nanoparticle conjugates for the photodynamic therapy of amelanotic melanoma. *European journal of cancer* **46**, 1910-1918 (2010).

88 Jang, B., Park, J.-Y., Tung, C.-H., Kim, I.-H. & Choi, Y. Gold nanorod− photosensitizer complex for near-infrared fluorescence imaging and photodynamic/photothermal therapy in vivo. *ACS nano* **5**, 1086-1094 (2011).

89 Gao, L. *et al.* Hypocrellin-loaded gold nanocages with high two-photon efficiency for photothermal/photodynamic cancer therapy in vitro. *Acs Nano* **6**, 8030-8040 (2012).

90 Seo, S.-H. *et al.* NIR-light-induced surface-enhanced Raman scattering for detection and photothermal/photodynamic therapy of cancer cells using methylene blue-embedded gold nanorod@ SiO2 nanocomposites. *Biomaterials* **35**, 3309-3318 (2014).

91 Mikhaylov, G. *et al.* Ferri-liposomes as an MRI-visible drug-delivery system for targeting tumours and their microenvironment. *Nature nanotechnology* **6**, 594 (2011).

92 Ke, F. *et al.* Facile fabrication of magnetic metal–organic framework nanocomposites for potential targeted drug delivery. *Journal of Materials Chemistry* **21**, 3843-3848 (2011).

93 Huang, P. *et al.* Photosensitizer-conjugated magnetic nanoparticles for in vivo simultaneous magnetofluorescent imaging and targeting therapy. *Biomaterials* **32**, 3447-3458 (2011).

94 Van Dongen, G., Visser, G. & Vrouenraets, M. Photosensitizer-antibody conjugates for detection and therapy of cancer. *Advanced drug delivery reviews* **56**, 31-52 (2004).

95 Bullous, A. J., Alonso, C. M. & Boyle, R. W. Photosensitiser–antibody conjugates for photodynamic therapy. *Photochemical & Photobiological Sciences* **10**, 721-750 (2011).

96 Mew, D., Wat, C.-K., Towers, G. & Levy, J. Photoimmunotherapy: treatment of animal tumors with tumor-specific monoclonal antibody-hematoporphyrin

conjugates. *The Journal of Immunology* **130**, 1473-1477 (1983).

97 Rai, P. *et al.* Development and applications of photo-triggered theranostic agents. *Advanced drug delivery reviews* **62**, 1094-1124 (2010).

98 Celli, J. P. *et al.* Imaging and photodynamic therapy: mechanisms, monitoring, and optimization. *Chemical reviews* **110**, 2795-2838 (2010).

99 Rosenthal, I., Sostaric, J. Z. & Riesz, P. Sonodynamic therapy—a review of the synergistic effects of drugs and ultrasound. *Ultrasonics sonochemistry* **11**, 349-363 (2004).

100 Norum, O. J. *et al.* Photochemical internalization of bleomycin is superior to photodynamic therapy due to the therapeutic effect in the tumor periphery. *Photochemistry and photobiology* **85**, 740-749 (2009).

101 Jerjes, W., Upile, T., Radhi, H. & Hopper, C. Photodynamic therapy vs. photochemical internalization: the surgical margin. *Head & neck oncology* **3**, 53 (2011).

102 Benov, L. Photodynamic therapy: current status and future directions. *Medical Principles and Practice* **24**, 14-28 (2015).

103 Thurber, G. M., Schmidt, M. M. & Wittrup, K. D. Antibody tumor penetration: transport opposed by systemic and

antigen-mediated clearance. *Advanced drug delivery reviews* **60**, 1421-1434 (2008).

104 Weis, S. M. & Cheresh, D. A. Tumor angiogenesis: molecular pathways and therapeutic targets. *Nature medicine* **17**, 1359-1370 (2011).

105 Li, Z.-b. *et al.* 64Cu-labeled tetrameric and octameric RGD peptides for small-animal PET of tumor αvβ3 integrin expression. *Journal of Nuclear Medicine* **48**, 1162-1171 (2007).

106 Jin, Z.-H. *et al.* In vivo optical imaging of integrin α V-β 3 in mice using multivalent or monovalent cRGD targeting vectors. *Molecular cancer* **6**, 41 (2007).

107 Dijkgraaf, I. *et al.* Improved targeting of the αvβ3 integrin by multimerisation of RGD peptides. *European journal of nuclear medicine and molecular imaging* **34**, 267-273 (2007).

108 Li, Z.-B., Chen, K. & Chen, X. 68Ga-labeled multimeric RGD peptides for microPET imaging of integrin αvβ3 expression. *European journal of nuclear medicine and molecular imaging* **35**, 1100-1108 (2008).

109 Schottelius, M., Laufer, B., Kessler, H. & Wester, H.-J. r. Ligands for mapping αvβ3-integrin expression in vivo. *Accounts of chemical research* **42**, 969-980 (2009).

110 Wu, Y. *et al.* microPET imaging of glioma integrin αvβ3 expression using 64Cu-labeled tetrameric RGD peptide. *Journal of Nuclear Medicine* **46**, 1707-1718 (2005).

111 Rudnick, S. I. & Adams, G. P. Affinity and avidity in antibody-based tumor targeting. *Cancer Biotherapy and Radiopharmaceuticals* **24**, 155-161 (2009).

112 Morlieras, J. *et al.* Functionalization of small rigid platforms with cyclic RGD peptides for targeting tumors overexpressing αvβ3-integrins. *Bioconjugate chemistry* **24**, 1584-1597 (2013).

113 Takemoto, H. *et al.* Accelerated polymer–polymer click conjugation by freeze–thaw treatment. *Bioconjugate chemistry* **23**, 1503-1506 (2012).

114 Wang, Y. *et al.* Optimization of RGD-containing cyclic peptides against αvβ3 integrin. *Molecular cancer therapeutics* **15**, 232-240 (2016).

115 Jin, J., Krishnamachary, B., Mironchik, Y., Kobayashi, H. & Bhujwalla, Z. M. Phototheranostics of CD44-positive cell populations in triple negative breast cancer. *Scientific reports* **6**, 27871 (2016).

116 Moan, J. & BERG, K. The photodegradation of porphyrins in cells can be used to estimate the lifetime of singlet oxygen.

Photochemistry and photobiology **53**, 549-553 (1991).

117 Fujimori, K., Covell, D. G., Fletcher, J. E. & Weinstein, J. N. A modeling analysis of monoclonal antibody percolation through tumors: a binding-site barrier. *Journal of nuclear medicine: official publication, Society of Nuclear Medicine* **31**, 1191-1198 (1990).

118 Wängler, C. *et al.* Multimerization of cRGD peptides by click chemistry: synthetic strategies, chemical limitations, and influence on biological properties. *ChemBioChem* **11**, 2168-2181 (2010).

119 Alam, M. R. *et al.* Multivalent cyclic RGD conjugates for targeted delivery of small interfering RNA. *Bioconjugate chemistry* **22**, 1673-1681 (2011).

120 Garanger, E., Boturyn, D., Coll, J.-L., Favrot, M.-C. & Dumy, P. Multivalent RGD synthetic peptides as potent α V β 3 integrin ligands. *Organic & biomolecular chemistry* **4**, 1958-1965 (2006).

121 Hersel, U., Dahmen, C. & Kessler, H. RGD modified polymers: biomaterials for stimulated cell adhesion and beyond. *Biomaterials* **24**, 4385-4415 (2003).

122 Chen, X. *et al.* Micro-PET imaging of αvβ3-integrin expression with 18F-labeled dimeric RGD peptide. *Molecular*

imaging **3**, 153535002004041O9 (2004).

123 Lucie, S. *et al.* Clustering and internalization of integrin αvβ3 with a tetrameric RGD-synthetic peptide. *Molecular therapy* **17**, 837-843 (2009).

124 Miura, Y. *et al.* Cyclic RGD-linked polymeric micelles for targeted delivery of platinum anticancer drugs to glioblastoma through the blood–brain tumor barrier. *ACS nano* **7**, 8583-8592 (2013).

125 Quader, S. *et al.* cRGD peptide-installed epirubicin-loaded polymeric micelles for effective targeted therapy against brain tumors. *Journal of Controlled Release* **258**, 56-66 (2017).

126 Jiang, X. *et al.* Integrin-facilitated transcytosis for enhanced penetration of advanced gliomas by poly (trimethylene carbonate)-based nanoparticles encapsulating paclitaxel. *Biomaterials* **34**, 2969-2979 (2013).

127 Jain, R. K. & Stylianopoulos, T. Delivering nanomedicine to solid tumors. *Nature reviews Clinical oncology* **7**, 653-664 (2010).

128 Lucky, S. S., Soo, K. C. & Zhang, Y. Nanoparticles in photodynamic therapy. *Chemical reviews* **115**, 1990-2042 (2015).

129 Maeda, H., Nakamura, H. & Fang, J. The EPR effect for

macromolecular drug delivery to solid tumors: Improvement of tumor uptake, lowering of systemic toxicity, and distinct tumor imaging in vivo. *Advanced drug delivery reviews* **65**, 71-79 (2013).

130 Song, C. *et al.* Enhanced Nanodrug Delivery to Solid Tumors Based on a Tumor Vasculature‐Targeted Strategy. *Advanced Functional Materials* **26**, 4192-4200 (2016).

131 Kibria, G., Hatakeyama, H., Ohga, N., Hida, K. & Harashima, H. The effect of liposomal size on the targeted delivery of doxorubicin to Integrin αvβ3-expressing tumor endothelial cells. *Biomaterials* **34**, 5617-5627 (2013).

132 Li, F., Zhao, Y., Mao, C., Kong, Y. & Ming, X. RGD-Modified Albumin Nanoconjugates for Targeted Delivery of a Porphyrin Photosensitizer. *Molecular Pharmaceutics* **14**, 2793-2804 (2017).

133 Spring, B. Q. *et al.* A photoactivable multi-inhibitor nanoliposome for tumour control and simultaneous inhibition of treatment escape pathways. *Nature nanotechnology* **11**, 378 (2016).

Achievements

Publications

1. Dou, X., Nomoto, T., Takemoto, H., Matsui, M., Tomoda, K. & Nishiyama, N.

Effect of multiple cyclic RGD peptides on tumor accumulation and intratumoral distribution of IRDye 700DX-conjugated polymers. *Scientific Reports volume 8, Article number: 8126 (2018)*

Conference

1. Xuebo Dou, Takahiro Nomoto, Hiroyasu Takemoto, Makoto Matsui, Keishiro Tomoda and Nobuhiro Nishiyama

"Effect of multiple cyclic RGD peptides on tumor accumulation and intratumoral distribution of photosensitizer-conjugated polymers"

66th Symposium on Macromolecules, Ehime.